



1 **INTERSEISMIC AND LONG-TERM DEFORMATION OF SOUTHEASTERN**
2 **SICILY DRIVEN BY THE IONIAN SLAB ROLL-BACK**

3 **Amélie Viger^{1*}, Stéphane Dominguez^{1*}, Stéphane Mazzotti¹, Michel Peyret¹, Maxime Henri-**
4 **quet², Giovanni Barreca^{3*}, Carmelo Monaco³, Adrien Damon¹**

(1) Géosciences Montpellier, Université de Montpellier, CNRS, Montpellier, France

(2) Aix-Marseille Université, CEREGE, Aix-en-Provence, France

(3) Dipartimento di Scienze Biologiche, Geologiche e Ambientali, Sezione di Scienze della Terra, Università di Catania, Catania, Italy

*e-mail, amelie.viger.geo@gmail.com, stephane.dominguez@umontpellier.fr, giobarre@unict.it

5 **Key Points**

- 6 • Recent satellite geodetic data shed new light on the origin of the active
7 deformations affecting Southeastern Sicily.
- 8 • Several deformation processes, including crustal flexure and faulting, are
9 investigated to determine the most reliable mechanical explanation.
- 10 • Seismic cycle, surface, and crustal deformations of Southeastern Sicily are mainly
11 driven by the southward migration of the Ionian slab roll-back.

12 **Abstract:**

13 New satellite geodetic data challenge our knowledge of the deformation mechanisms dri-
14 ving the active deformations affecting Southeastern Sicily. The PS-InSAR measurements
15 evidence a generalized subsidence and an eastward tilting of the Hyblean Plateau combi-
16 ned with a local relative uplift along its eastern coast. In order to find a mechanical expla-
17 nation for the present-day strain field, we investigate short and large-scale surface-to-crus-
18 tal deformation processes. Geological and geophysical data suggest that the southward
19 migration of the Calabrian subduction could be the causative geodynamic process. We
20 evaluate this hypothesis using flexural modeling and show that the overloading of the Ca-
21 labrian accretionary prism, combined with the downward pull force induced by the Ionian
22 slab roll-back, are capable of flexuring the adjacent Hyblean continental crust, explaining



23 the measured large-scale subsidence and eastward bending of the Hyblean Plateau. To
24 explain the short-scale relative uplift evidenced along the eastern coast, we perform elastic
25 modeling on identified or inferred onshore and offshore normal faults. We also investigate
26 the potential effects of other deformation processes including upwelling mantle flow, volca-
27 nic deflation, and hydrologic loading. Our results enable us to propose an original seismic
28 cycle model for Southeastern Sicily, linking the current interseismic strain field and the
29 available long-term deformation data. This model is mainly driven by the southward migra-
30 tion of the Ionian slab roll-back which induces a downward force capable to flexure the Hy-
31 blean crust.

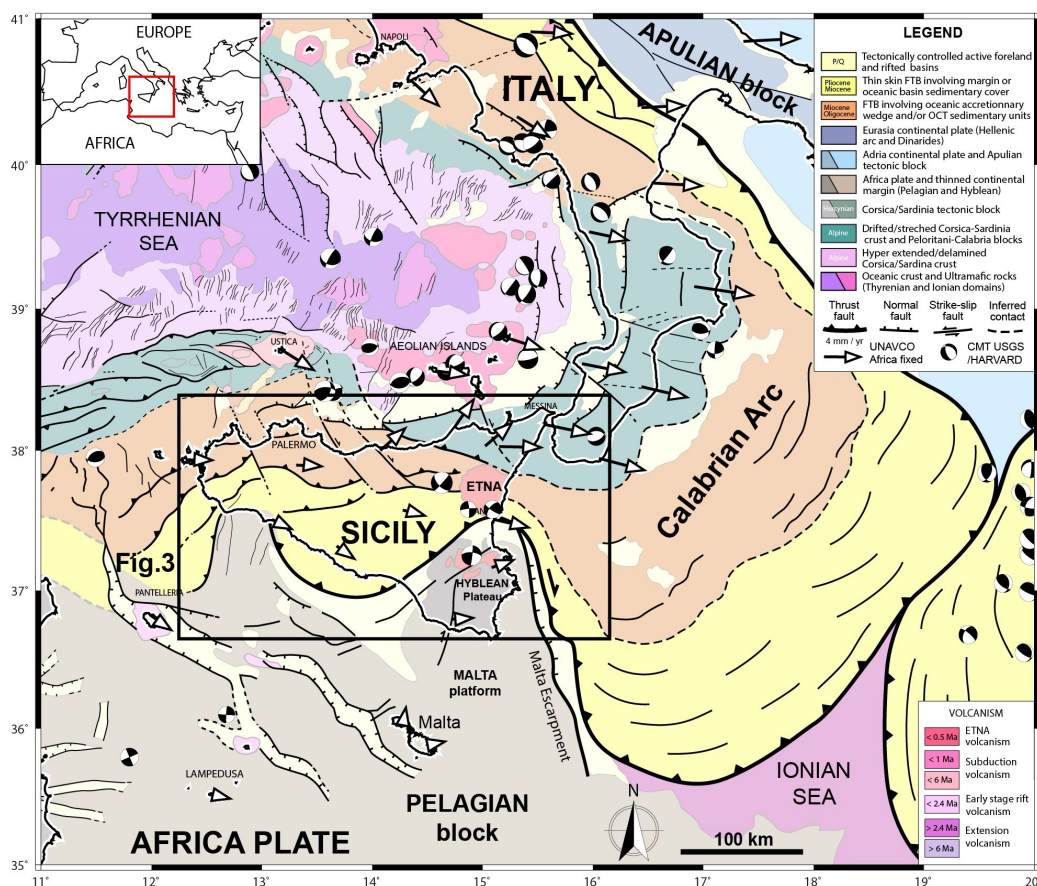
32 **Keywords:** Southeastern Sicily, surface deformation, PS-InSAR, slab roll-back, slab pull,
33 crustal/lithospheric flexure, extrado faulting, seismic cycle, numerical modeling

34 1. Introduction

35 Geodetic measurements, instrumental seismicity, onshore/offshore geology, and
36 geophysics, all indicate that Southeastern Sicily is actively deforming (e.g., Anzidei *et al.*,
37 2021; Azzaro and Barbano, 2000; Mastrolembo *et al.*, 2014; Meschis *et al.*, 2020). This re-
38 gion also suffered the most powerful and devastating earthquake reported in the Italian
39 seismicity catalog, the 1693 Mw~7.4 Val-di-Noto earthquake, which occurred along the
40 eastern margin of the Hyblean Plateau (e.g., Bianca *et al.*, 1999; Billi *et al.*, 2010; Gutscher
41 *et al.*, 2006; Scicchitano *et al.*, 2022). The current geologic and tectonic framework is in
42 line with the Cenozoic geodynamic evolution of the Central Mediterranean (Figure 1), but
43 also appears to be influenced by the Mesozoic pre-structuration of this region (e.g., Carmi-
44 nati and Doglioni, 2005; Frizon de Lamotte *et al.*, 2011; Henriquet *et al.*, 2020; Van Hins-
45 bergen *et al.*, 2020). In the Late Cretaceous (~80 Myr), the Africa/Eurasia plates conver-



46 gence initiated the oceanic subduction of the Alpine Tethys under the Apulia-Adria micro-
47 continent (e.g., Handy *et al.*, 2010). Since the Oligocene (~30 Myr), the Alpine Tethys sub-
48 duction has experienced slab roll-back, causing the drifting of continental micro-blocks, de-
49 tached from the Iberia plate and the opening of back-arc basins over the Mediterranean
50 realm (e.g., Carminati *et al.*, 2012; Gueguen *et al.*, 1998; Rosenbaum *et al.*, 2002). During
51 the Mio-Pliocene (10-5 Myr), the collision of the retreating Calabrian-Peloritan subduction
52 arc and accretionary wedge with the Northern African passive margin led to the formation
53 of the Sicilian fold-and-thrust belt (e.g., Henriquet *et al.*, 2020). During the Plio-Pleistocene
54 (5-2 Myr), the Calabrian subduction continued strongly interacting with the crustal structure
55 of the African margin, in particular with the thick Pelagian continental lithosphere, the Malta
56 Escarpment, and the Ionian oceanic lithosphere (Wortel and Spakman, 2000) (Figure 1).
57 These three major tectonic domains, which originated during the Triassic period, were
58 shaped by the fragmentation of the Pangea in the early Jurassic, leading to the opening of
59 the Neo-Tethys Ocean (e.g., Stampfli *et al.*, 2002). Nowadays, the Calabrian subduction
60 zone keeps moving south but at a much slower rate, suggesting that the whole system is
61 subjected to opposing forces and/or that its driving mechanism, slab roll-back, is losing ef-
62 ficiency.



63 **Figure 1:** Geodynamic and tectonic map of Central Mediterranean (modified from Henriquet *et al.*, 2020).
64 Geological data were synthesized from large-scale maps (e.g., Funicello *et al.*, 1981; Bigi *et al.*, 1991; APAT,
65 2005; Lentini and Carbone, 2014). Structural data were synthesized from previous publications (e.g., Finetti
66 *et al.*, 2005; Chamot-Rooke *et al.*, 2005; Corti *et al.*, 2006; Prada *et al.*, 2014; Lymer *et al.*, 2018; Rabaute
67 and Chamot-Rooke, 2019). Present-day Centroid Moment Tensors ($M_w > 4.5$) and GNSS data were re-
68 trieved from <https://www.globalcmt.org/CMTsearch.html> and <https://www.unavco.org/data/gps-gnss/gps-gnss.html>
69 websites, respectively.

70 Recent PS-InSAR satellite measurements (radar interferometry), published by Hen-
71 riquet *et al.* (2022), have revealed an unexpected pattern of surface deformation across
72 Southeastern Sicily, in particular, an eastward increasing subsidence of the whole Hyblean
73 Plateau (Figure 2). This region has been partially investigated in previous studies, using si-
74 milar techniques, but only captured local surface deformation features (Canova *et al.*,
75 2012; Vollrath *et al.*, 2017). Up to now, the origin of such a pattern of deformation remains,



76 then, unexplained. Since satellite measurements were acquired over a very short period
77 compared to typical seismic cycle durations (five versus several hundreds of years), and
78 considering the discrepancy between satellite measurements and inferred long-term coastal
79 uplift estimations (e.g., Bianca *et al.*, 1999; Ferranti *et al.*, 2006, 2010; Meschis *et al.*,
80 2020; Scicchitano *et al.*, 2008) (Figure 2a), we hypothesize that the satellite data are re-
81 presentative of the interseismic period. We further infer that the PS-InSAR data mainly do-
82 cument elastic loading mechanisms and reversible deformations. To explain the geodetic
83 observations, we investigate the surface deformation signature of crustal and lithospheric
84 deformation processes, including the impact of the southward migration of the Calabrian
85 subduction system on the structural evolution of the eastern Hyblean margin as well as
86 elastic loading and aseismic creep on coastal and offshore normal faults. We also test the
87 potential surface expression of other processes such as volcanic deflation, hydrologic loa-
88 ding, and upwelling mantle flow.

89 **2. Present-day deformation of SE Sicily**

90 The kinematics and active tectonics in the SE Sicily are still a matter of debate, with
91 major evolutions in the last decade (e.g., Argnani *et al.*, 2012; Bianca *et al.*, 1999), in parti-
92 cular with the acquisition of high-resolution bathymetry and seismic profiles in the adjacent
93 Ionian domain (Dellong *et al.*, 2020; Gambino *et al.*, 2021, 2022; Gutscher *et al.*, 2016; Ri-
94 dente *et al.*, 2014). Main reasons include the complex polyphased geological history of this
95 region and the relatively low present-day horizontal strain rate (< 5 mm/yr), resulting from
96 the slowdown of the Calabrian subduction zone activity in the last million years (Goes *et*
97 *al.*, 2004).

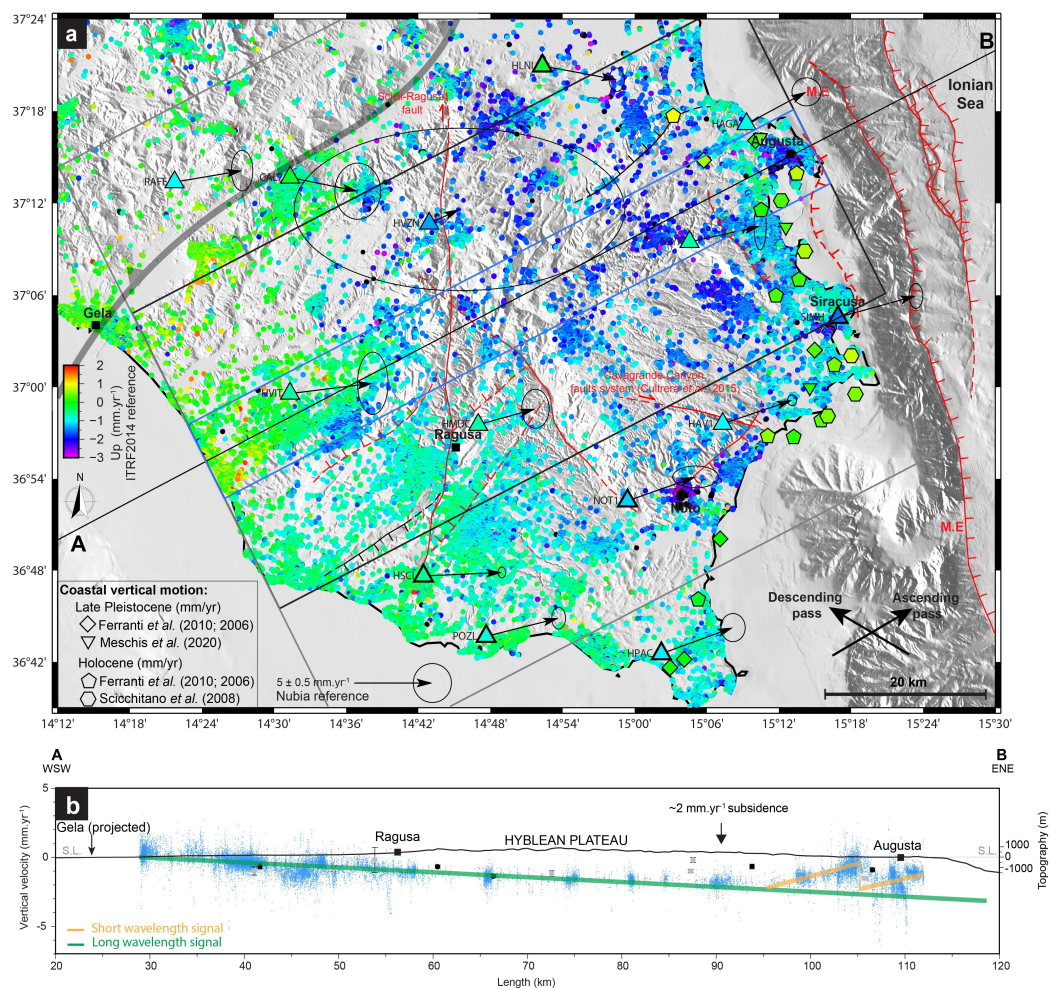
98 **2.1 Geodesy**



99 Geodetic surface measurements in SE Sicily include GNSS (e.g., Palano *et al.*,
100 2012), PS-InSAR/DInSAR (e.g., Vollrath *et al.*, 2017), and leveling datasets (e.g., Spampi-
101 nato *et al.*, 2013).

102 **PS-InSAR**

103 In the present study, we use the first geodetic velocity field covering the whole Island of
104 Sicily published by Henriquet *et al.* (2022) and derived from Sentinel-1 radar satellite (In-
105 SAR data) acquired during the 2015-2020 period. The PS-InSAR pseudo-3D velocity field
106 (Up and E-W component) was obtained by merging ascending and descending acquisi-
107 tions, combined with a reanalysis of the GNSS time series. Due to the acquisition geome-
108 try, Sentinel-1 radar satellite is not sensitive to the N-S component of horizontal surface
109 deformation, which is, fortunately, very low in the studied region (Henriquet *et al.*, 2022).
110 We therefore consider that, even if affected by minor distortions, the Up and E-W compo-
111 nents of the pseudo-3D velocity data can be used with confidence (Supplementary Figures
112 S2 to S5). The vertical (Up) component of this dataset reveals that the central and eastern
113 parts of the Hyblean Plateau experience subsiding rates increasing eastward from 1 to
114 nearly 3 mm/yr relative to the western coast (Figure 2). It should be noted that PS-InSAR
115 data also show a slowly decreasing E-W component to the east of the Hyblean Plateau
116 with velocities evolving from 3 to 2 mm/yr (fig.10, Henriquet *et al.*, 2022).



117 **Figure 2:** Geodetic data across the Hyblean Plateau region (see location in Figure 3). The Permanent-Scat-
 118 terer (PS-InSAR) pseudo-3D Up velocities are from Henriquet et al. (2022) and are measured during the
 119 2015-2020 period. GNSS 3D surface velocities are derived from a reanalysis of the Nevada Geodetic Labo-
 120 ratory (NGL) (Horizontal components reference: fixed Nubia; Up components reference: ITRF2014). Major
 121 faults of the Hyblean Plateau and Malta Escarpment (M.E) including the offshore normal faults identified by
 122 Gutscher et al. (2016) and analyzed by Gambino et al. (2021) (red: active fault; red dashed: inferred active
 123 fault; black: inferred aseismic slip (Spampinato et al., 2013)). SW-NE trending velocity profile showing sur-
 124 face velocity (Up) derived from PS-InSAR and GNSS stations vertical velocities. PS-InSAR data are stacked
 125 across a 5 km width on both sides of the AB profile (in blue). GNSS data are stacked using 20 km (in black)
 126 and 40 km (in gray) widths on both sides of the AB profile. Topographic and bathymetric profiles are pre-
 127 sented without vertical exaggeration (V.E.x1).

128 One should note that the zero reference of the PS-InSAR vertical velocity field is not
 129 precisely known. The vertical component of the pseudo-3D PS-InSAR velocity field and



130 GNSS data have a ± 0.5 mm/yr uncertainty in the ITRF2014 (Altamimi *et al.*, 2016), which
131 implies that the observed subsidence over the Hyblean Plateau could be a little bit higher
132 or slower. In the last case, slow uplift rates could be present in the Gela region. The verti-
133 cal velocity trend is obtained by projecting and stacking the PS-InSAR data across a 5 km
134 wide band along a N30°E AB profile (Figure 2b). Along this profile, oriented perpendicular
135 to the main regional faults, the subsidence velocity reaches, in average, ~ 1 mm/yr be-
136 tween Gela and Ragusa and increases progressively to ~ 2.5 mm/yr between Ragusa and
137 Augusta.

138 All along the eastern coast, a significant slower subsidence (or a relative uplift) is
139 observed. From Augusta to Siracusa, and in the southernmost part of the Hyblean Plateau
140 (HP), the subsidence rate decreases to about 1 mm/yr compared to the maximum subsi-
141 dence rate in the central Hyblean Plateau (Figure 2). In the Gela region, PS-InSAR vertical
142 velocities indicate a possible slow uplift rate of ~ 0.5 mm/yr (Figure 2). A second profile, lo-
143 cated 20 km south of the AB profile shows the same eastward increase of the subsidence
144 rates, evolving towards a similar relative uplift in the Siracusa region (Supplementary Fig-
145 ure S1).

146 Along the AB velocity profile, nor the Scicli-Ragusa inferred active fault (Vollrath *et*
147 *al.*, 2017), nor the other major faults of the Hyblean Plateau can be evidenced in both the
148 E-W and vertical components of the PS-InSAR data (Henriquet *et al.*, 2022) (Figure 2a),
149 indicating that these faults are locked or are creeping at a slip rate lower than the PS-In-
150 SAR resolution (± 0.5 mm/yr). Locally, fast (> 3 mm/yr) subsiding zones, most probably re-
151 lated to human activities such as water pumping (Canova *et al.*, 2012), can be identified
152 near the main cities of Augusta, Siracusa and Noto (Figure 2a).

153 Surface deformations signals extending over a hundred or more kilometers are
154 most probably related to crustal or lithospheric scale processes (e.g., Stephenson *et al.*,
155 2022), whereas those extending over tens of kilometers are likely associated with much



156 shallower and localized mechanical processes such as, seismic cycle deformation,
157 volcanic bulging/collapse, hillslope instabilities (landslides), or human activities (water
158 pumping, mining) (e.g., Vilaro *et al.*, 2009). We therefore hypothesize that the PS-InSAR
159 vertical velocity field consists of two superimposed signals: (1) a long wavelength (> 100
160 km) subsidence, and gradual eastward tilt of the Hyblean Plateau (green line in Figure 2b),
161 compatible with the decreasing PS-InSAR E-W velocities, and (2) a short wavelength si-
162 gnal, extending along the Eastern coast and characterized by sharp variations of the verti-
163 cal velocities at kilometric scale (orange lines in Figure 2b).

164 **GNSS**

165 The Global Navigation Satellite System (GNSS) data used to calibrate the pseudo-3D PS-
166 InSAR velocity field (Henriquet *et al.*, 2022) were based on the analysis of time series, re-
167 trieved from the Nevada Geodetic Laboratory (Blewitt *et al.*, 2018). We refine this analysis
168 by correcting for annual and semiannual seasonal signals, instantaneous offsets, and
169 gaps, using the time series inversion software developed by Masson *et al.* (2019). Across
170 the Hyblean Plateau, GNSS velocities show horizontal velocities of ~ 2 mm/yr oriented ho-
171 mogeneously toward the ENE, in the Nubia reference frame (Figure 2). The vertical com-
172 ponent of most of the GNSS stations shows an overall subsidence of the HP (-0.8 mm/yr
173 in average) in the ITRF2014 reference frame (Altamimi *et al.*, 2016). This tendency is well
174 illustrated by the high-quality NOT1 GNSS station located near the city of Noto, which has
175 recorded the longest time series (23 years, 2000-2023), or by the SSYX and HMDC sta-
176 tions (Supplementary Figures S2 and S3). Overall, the GNSS vertical velocities are consis-
177 tent with the median of the PS-InSAR vertical velocities calculated over an 8 km^2 region
178 centered on each GNSS station (Supplementary Figures S2 to S5).

179 We used, then, this GNSS dataset to estimate a regional horizontal strain rate ten-
180 sor, using the inversion model of Mazzotti *et al.*, 2005. The Hyblean Plateau is character-

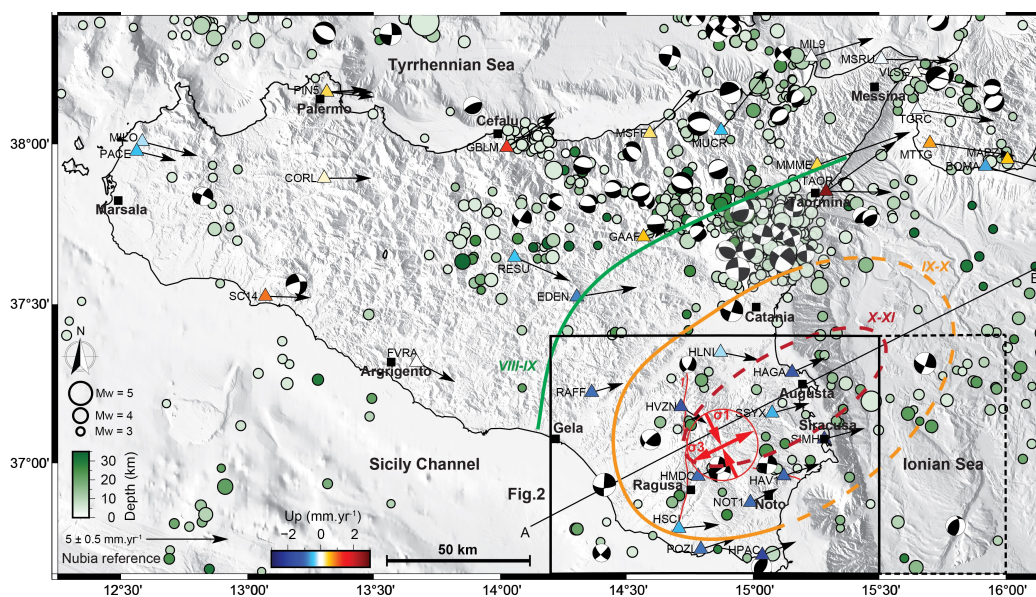


181 ized by an extension rate oriented SW-NE and a shortening rate oriented N165°E (Supple-
182 mentary Figure S6), consistent with the focal mechanisms inversion (*Figure 3*).

183 **2.2 Seismology**

184 The instrumental seismicity map of SE Sicily, derived from INGV and Rovida *et al.*
185 (2022) datasets (*Figure 3*), shows minor to moderate events ($M < 5$) with deep crustal
186 hypocenters (15-30 km). Over the Hyblean Plateau, earthquake hypocenters tend to
187 roughly align along the inferred active, N-S trending, Scicli-Ragusa strike-slip fault (e.g.,
188 Vollrath *et al.*, 2017) and near the Cavagrando Canyon faults system (Cultrera *et al.*, 2015)
189 (*Figure 3*). Most of these faults are probably inherited from the Plio-Quaternary tectono-
190 magmatic phase of deformation (Henriquet *et al.*, 2019), and were partly re-activated in re-
191 sponse to the ongoing Africa-Nubia/Eurasia plates convergence (e.g., Cultrera *et al.*, 2015;
192 Mattia *et al.*, 2012). In this framework, the identification of the seismogenic source that trig-
193 gered the 1693 event remains debated (e.g., Bianca *et al.*, 1999; Argnani and Bonazzi,
194 2005). The isoseists of $M_w \sim 7.4$ Noto earthquake appear largely open toward the Malta Es-
195 carpment and Ionian Sea domains, suggesting the seismogenic faults could be located off-
196 shore (*Figure 3*). East of the Hyblean Plateau, earthquakes essentially distribute along the
197 Malta Escarpment where a normal fault system, potentially responsible for the 1693 earth-
198 quake, has been identified (e.g., Bianca *et al.*, 1999; Gutscher *et al.*, 2016; Gambino *et al.*,
199 2021, 2022), (*Figure 3*).

200 The focal mechanisms over the Hyblean Plateau have dominant strike-slip charac-
201 teristics, contrasting with the extensive deformation characterizing the NE corner of Sicily
202 (*Figure 3*).



203 **Figure 3:** Instrumental seismicity of Sicily at crustal scale (0-30 km depth) showing earthquake hypocentral
204 locations and focal mechanism solutions of $M>3$ events from 1985 to 2022 (Istituto Nazionale di Geofisica e
205 Vulcanologia (INGV), 2005; Scognamiglio *et al.*, 2006). 3D surface velocity derived from GNSS time series
206 published in Henriquet *et al.* (2022) (Horizontal components reference: fixed Nubia; Up components refer-
207 ence: ITRF2014). Macroseismic intensity data of the 1693 Val-di-Noto Earthquake ($M\sim 7.4$) from INGV
208 CPT115 database (Rovida *et al.*, 2022): red dashed line = X-XI intensity, orange dashed line = IX-X intensity,
209 green dashed line = VIII-IX intensity). Focal mechanisms stress inversion (red arrows) for the Hyblean
210 Plateau region (black frame) and Ionian Sea (black dashed frame) using Michael's method (Vavryčuk, 2014;
211 Levandowski *et al.*, 2018). The AB profile shows the location of the PS-InSAR profile and synthetic structural
212 cross-section presented in Figures 2 and 4.

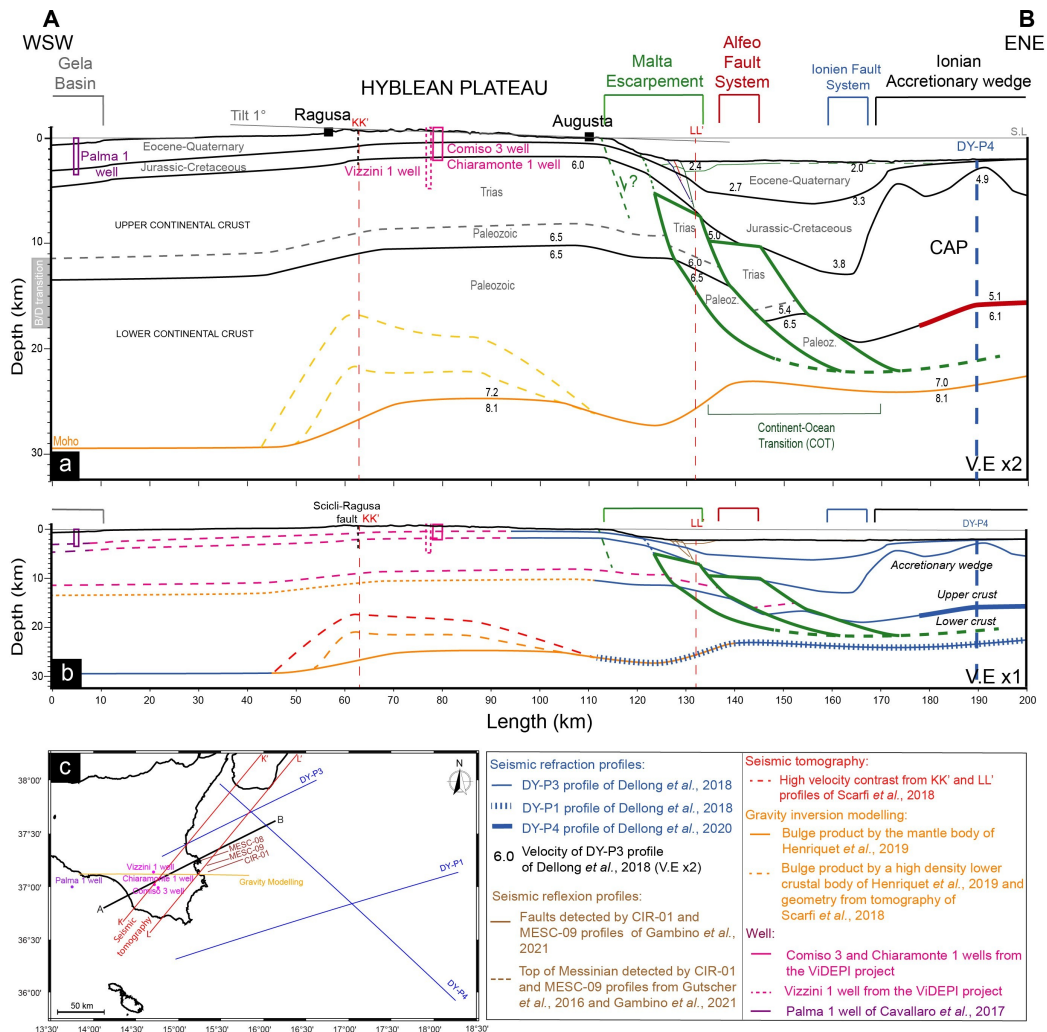
213 To estimate the present-day regional stress field across SE Sicily, we use the
214 Vavryčuk's numerical model (Vavryčuk, 2014; Levandowski *et al.*, 2018), based on
215 Michael's method (Michael, 1984). Results show that the regional stress across SE Sicily
216 (Figure 3) is homogeneous (Supplementary Figures S7 and S8). The maximum compres-
217 sive stress (σ_1) is horizontal and oriented $N154^\circ E \pm 7^\circ$, compatible with the $N160^\circ E$ Africa-
218 Eurasia plates convergence (e.g., Mattia *et al.*, 2012; Kremer *et al.*, 2014). The minimum
219 stress (σ_3) is oriented $N64^\circ E \pm 7^\circ$, compatible with the GNSS extension rate (Figure 3).



220 This regional stress field is compatible with the measured geodetic surface defor-
221 mation (E-W extension) but does not explain the observed eastward-increasing subsi-
222 dence rate across the HP.

223 **2.3 Synthetic structural profile**

224 To better constrain the deep structure and rheology of the studied area, we synthe-
225 size the available geological, and geophysical data into a 200 km long simplified crustal-
226 scale structural cross-section following the N30°E AB profile crossing the Hyblean Plat-
227 form, the Malta Escarpment, the western Ionian domain, and the offshore normal faults (Fi-
228 gures 2, 3 and 4). The eastern part of the synthetic structural profile is mainly based on
229 seismic refraction profiles from Dellong *et al.* (2018), particularly the DY-P3 profile running
230 sub-parallel to the AB profile and located 15 km further North, as well as seismic reflection
231 profiles from Argnani *et al.* (2012), Gutscher *et al.* (2016), and Gambino *et al.* (2021, 2022)
232 (Figure 4c). The structure of the western section is constrained by onshore and off-hore
233 geology, wells log stratigraphy, geophysics, seismic reflection profiles, and geological
234 cross-sections from the ViDEPI project, Cavallaro *et al.* (2017), Scarfi *et al.* (2018),
235 Henriquet *et al.* (2019) and Finetti *et al.* (2005).



236 **Figure 4:** Simplified crustal cross-section along the N30°E AB profile (see Figures 4c and 2 for location). a)
 237 Two times vertically exaggerated synthetic structural profile along with seismic velocity data showing the
 238 structure and rheology of the Hyblean Plateau and eastern oceanic domain determined from onshore and
 239 offshore geology, wells stratigraphy, geophysics, seismic reflection, and refraction profiles (see Legend for
 240 references). Note the 1° tilt of the Hyblean Plateau topography toward the East. The red line corresponds to
 241 the inferred position of the main subduction décollement, and the green lines, refer to our interpretation of
 242 tilted blocks from the Malta Escarpment (M.E). b) Synthetic structural profile along available data (see Leg-
 243 end) without vertical exaggeration (V.E.x1), showing the extent of the different datasets. c) Locations, in map
 244 view, of the AB profile, ViDEPI project wells data, tomography profile, refraction, and reflexion seismic pro-
 245 files.

246 In the Hyblean domain, geophysical data (e.g., SgROI *et al.*, 2012; Milano *et al.*,
 247 2020) indicate that the crust has an average thickness of ~30 km. Based on gravity data



248 modeling, Henriquet *et al.* (2019) evidenced a 100 km-large and 5 km-high lower crustal
249 body below the Hyblean Plateau, locally uplifting the Moho to a depth of about 20-25 km.
250 This feature is supported by tomographic data (Scarfì *et al.*, 2018). We constrain the geo-
251 metry of the Quaternary to Mesozoic sedimentary cover of the Hyblean Platform and Gela
252 basin using the Vizzini 1, Chiaramonte 1 and Comiso 3 wells (ViDEPI project) and the
253 Palma 1 well (Cavallaro *et al.*, 2017).

254 In the DY-P3 seismic refraction profile (Dellong *et al.*, 2018), the 6.0 and 6.5 km/s
255 velocity contours delimit two main steps deepening eastward at the junction between the
256 Hyblean continental and Ionian oceanic domains (Figures 4a and 4b). Considering their lo-
257 cations along the Malta Escarpment that outlines the continent-ocean transition (COT), we
258 interpret these velocity variations as deepening of the sediment/basement boundary, po-
259 tentially related to tilted blocks of thinned continental crust formed during the Triassic-Early
260 Jurassic rifting phase (see section 1) (e.g., Dellong *et al.*, 2018; Minelli and Faccenna,
261 2010; Scandone *et al.*, 1981; Tugend *et al.*, 2019).

262 As documented by Gutscher *et al.* (2016), and Gambino *et al.* (2021, 2022), the
263 seismic reflection profiles (CIR-01, MESC-08 and MESC-09) shows several normal faults
264 bounding and crossing the turbiditic valley, extending along the base of the Malta Escarp-
265 ment (Gutscher *et al.*, 2016). This turbiditic valley fault system is constituted by three major
266 parallel normal faults, 60 km long and dipping 35-50°E (Figures 4a and 4b), producing a
267 strong morphological offset of the Ionian seafloor from the latitudes of Catania to Siracusa
268 (cf. MESC-08 and MESC-09 seismic reflection profiles in Gambino *et al.*, 2021). We inter-
269 pret these offshore normal faults as potentially related to recent re-activation of the shallow
270 prolongation of the inferred Mesozoic tilted blocks (Figures 4a and 4b).

271 On the eastern side of the Hyblean domain, the Moho is constrained by DY-P3 and
272 DY-P1 refraction profiles to a depth of ~30 km below the Malta Escarpment. To the east, in



273 response to the bending of the Ionian slab, the Moho deepens northward from 20 km (DY-
274 P1) to 32 km (DY-P3). Based on these data and the DY-P4 refraction profile (Dellong *et al.*,
275 2020), we estimate the depth of the Moho below the Ionian oceanic crust to be about 20-
276 25 km in the eastern portion of the synthetic profile AB. In this region, the domain delimited
277 by the seismic refraction velocities of 4.9-5.1 km/s has been interpreted as corresponding
278 to the deformed sediments of the Calabrian accretionary prism (CAP) (Dellong *et al.*,
279 2018). Its thickness increases from 5 km (DY-P1) to 15 km (DY-P3), and it is evaluated to
280 be ~11 km along the AB profile (Figures 4a and 4b). Note that the Calabrian backstop (i.e.,
281 Hercynian basement) is not present in the AB profile (Figures 4a and 4b). The location of
282 the main subduction décollement along the AB profile has been estimated using the sharp
283 velocity step (5.1-6.1 km/s) seismic refraction DY-P3 and DY-P4 profiles (Dellong *et al.*,
284 2018) at a depth of 15-20 km (red line in Figure 4a).

285 **3. Mechanical model hypotheses**

286 To explain the long wavelength bending trend evidenced by the PS-InSAR velocity
287 Up component, we model the flexure of the Hyblean Plateau induced by (1) overloading of
288 the continent-ocean transition (COT) domain in response to the SE migration of the very
289 thick Calabrian accretionary prism (CAP), and (2) forced subsidence of the COT due to the
290 local increase of the slab pull force imposed by the southward roll-back of the Ionian sub-
291 duction. We hypothesize that these crustal/lithospheric deformation mechanisms may be
292 strong enough to induce the large-scale subsidence and tilt evidenced by the geodetic
293 data (PS-InSAR and GNSS) (Figure 2b). In addition, we test interseismic loading models
294 on several onshore and offshore east-dipping normal faults, such as the Augusta-Siracusa
295 fault, the Malta Escarpment, and the active faults documented by Gutscher *et al.* (2016)
296 and Gambino *et al.* (2021, 2022), to explain the short wavelength deformation signal ex-
297 tending along the eastern coast of the Hyblean Plateau (Figure 2b).

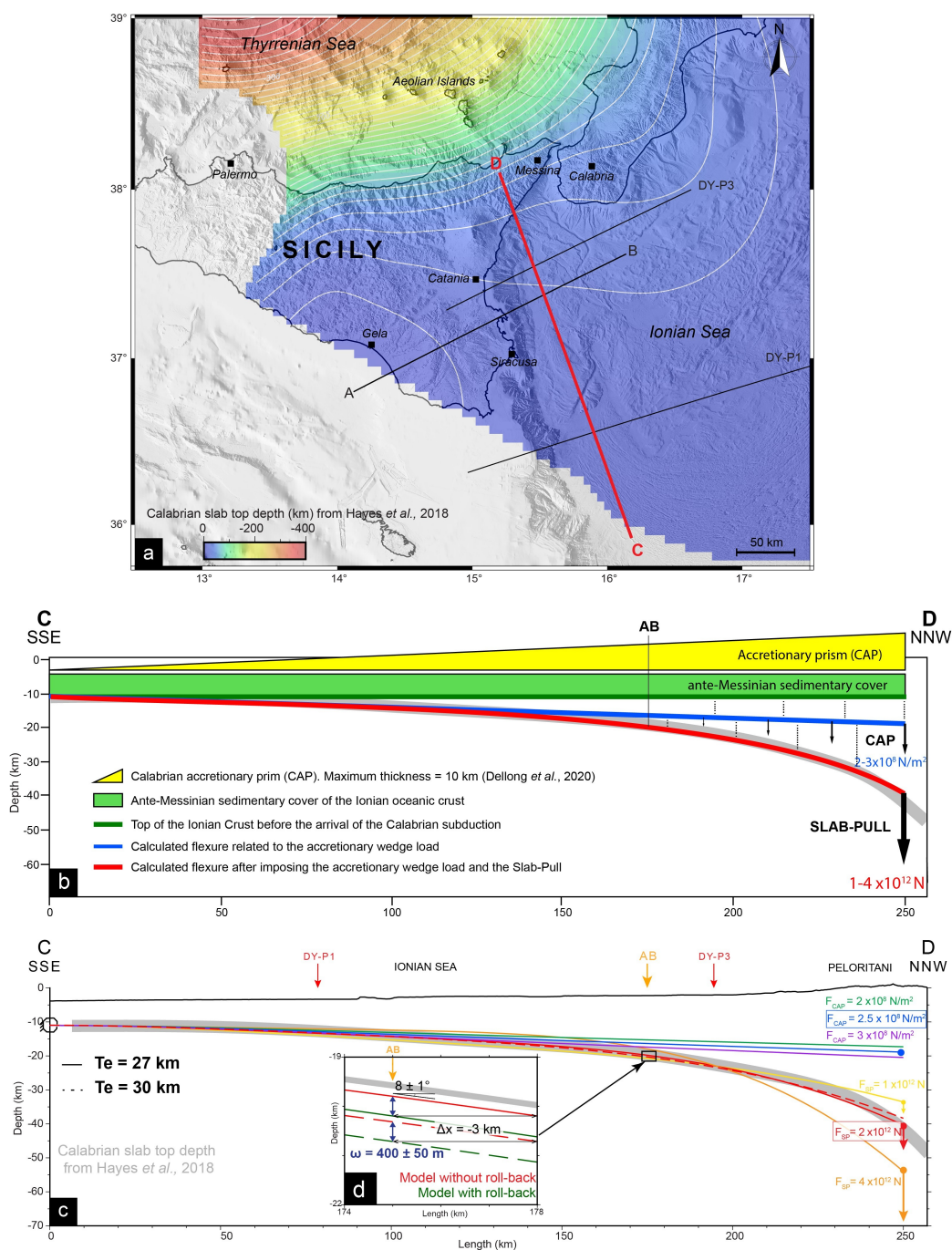


298 **3.1 Lithospheric flexure along a NNW-SSE profile**

299 To better constrain key flexural parameters, such as the rigidity of the Hyblean and
300 Ionian crust/lithospheres, the slab-pull force, and to investigate the impact of the Ionian
301 slab roll-back, we first model the bending of the subducting Ionian slab along a NNW-SSE
302 profile (CD profile), trending orthogonal to the AB profile (Figure 5a). As a structural refer-
303 ence, we use the isobaths of the top of the Ionian slab published by Hayes *et al.* (2018)
304 (Figure 5a).

305 The lithosphere flexure models (as well as those in section 3.2) are calculated using
306 the gFlex software (Wickert, 2016). We impose a no-displacement condition at the south-
307 ern profile boundary and a broken plate with no bending moment and no shear at the
308 northern boundary. The Ionian oceanic lithosphere is modeled assuming an effective elas-
309 tic thickness (T_e) ranging from 25 to 37 km (Figure 5b and Supplementary Figure S9),
310 compatible with its Permo-Triassic age (e.g., Catalano *et al.*, 2001; Speranza *et al.*, 2012)
311 and consistent with other publications (e.g., Watts and Zhong, 2000; Tesauro *et al.*, 2012;
312 Cloetingh *et al.*, 2015).

313 The flexure of the subducting slab depends on its mechanical properties and on the
314 loads induced by the sedimentary cover, the accretionary prism, and the slab pull force
315 (Figure 5b). According to seismic refraction profiles DY-P1 and DY-P3 (Dellong *et al.*,
316 2018), the undeformed ante-Messinian sedimentary cover overlying the Ionian crust has a
317 thickness of about 5 km. Thus, taking into account a depth of the Ionian Sea of 5-6 km, we
318 consider that the top of the Ionian crust was lying at a uniform depth of 10-11 km before
319 the onset of the Calabrian subduction system (Figure 5b). This depth corresponds to the
320 isostatic equilibrium for the Ionian crust. It determines the initial geometry of the flexural
321 model from which we calculate the bending induced by the Calabrian accretionary prism
322 (CAP) load.



323 **Figure 5:** a) Map and isobaths of the top of the Ionian slab subducting below the Calabrian Arc (data ex-
 324 tracted from Hayes et al., 2018). AB and CD profile locations are indicated, as well as seismic refraction pro-
 325 files DY-P3 and DY-P1 (Dellong et al., 2018). b) NNW-SSE trending CD cross-section (in gray) showing the
 326 flat and steep ramp geometry of the Ionian slab (see location in Figure 5a) following the CD profile in a. The
 327 Ionian oceanic lithosphere supports a 5 km thick homogeneous ante-Messinian sedimentary cover (in



328 green). The CAP thickness increases northward up to ~15 km (thickening of +10 km compared to the original
329 5 km thick undeformed sediment cover), according to Dellong *et al.* (2020) (in yellow), and the associated
330 flexure is represented in a blue line. The bending of the slab is controlled by the slab pull, represented as a
331 punctual load, ranging from $1-4 \times 10^{12}$ N, and added at the Ionian lithosphere flexure shown in a red line. c)
332 The ante-Messinian cover and the CAP load are performed with a maximum CAP load of 2×10^8 N/m² (green
333 line), 2.5×10^8 N/m² (blue line), or 3×10^8 N/m² (purple line). Flexural models are performed with different ef-
334 fective elastic thicknesses (T_e) ranging from 25 to 37 km (Supplementary Figure S9). We also consider elas-
335 tic thicknesses of 25 and 30 km (Supplementary Figure S9) to perform the flexural model with different slab
336 pull forces: 1×10^{12} N (yellow line), 2×10^{12} N (red line), and 4×10^{12} N (orange line). Topographic, slab, and
337 flexural model profiles are presented without vertical exaggeration (V.E.x1). d) Zoom of profiles CD and AB
338 intersection where the depth difference between favorite models, a CAP load of 2.5×10^8 N/m² and a slab pull
339 of 2×10^{12} N for an elastic thickness of 27 (continuous lines) and 30 (dashed line) km, without rollback (red
340 line) and with rollback (green line), has been calculated. The local subsidence associated with the 3 km/Myr
341 slab SE retreat is estimated to be about 400 ± 50 m.

342 Based on seismic refraction profiles DY-P4, DY-P1, and DY-P3 (Dellong *et al.*,
343 2018; 2020), the Calabrian accretionary prism thickness increases northward from 5 to 15
344 km. By removing the initial 5 km-thick Ionian sedimentary cover, the CAP load represents
345 an increase in sediment thickness from 0 km at the southern end of the CD profile to 10
346 km at its the northern end. The Calabrian backstop, made of Hercynian continental crust,
347 is not taken into account (Figure 5b).

348 The CAP load is calculated by:

$$349 \quad F_{CAP} = \rho g h \quad (1)$$

350 with a sediment density (ρ) of 2800 kg/m² (profile 2D) according to Dellong *et al.* (2020), a
351 gravity acceleration (g) of 9.81 m/s², and an increase of the CAP thicknesses (h) from 0 to
352 10 km.

353 The CAP load (F_{CAP}) is applied on the CD profile divided in 1-km-long segments by
354 imposing a northward linear gradient from 0 to 2.75×10^8 N/m² (equation 1) on the first 250
355 km of the profile (Figures 5b and 5c). We perform several tests with different maximum
356 CAP load (F_{CAP}) and elastic thicknesses (T_e) ranging from 2×10^8 to 3×10^8 N/m² and 25 to
357 37 km, respectively. Models are tested with a constant mantle density of 3300 kg/m² and
358 no filling density for mantle restoration force (Figure 5c). The resulting flexure (~8 km maxi-



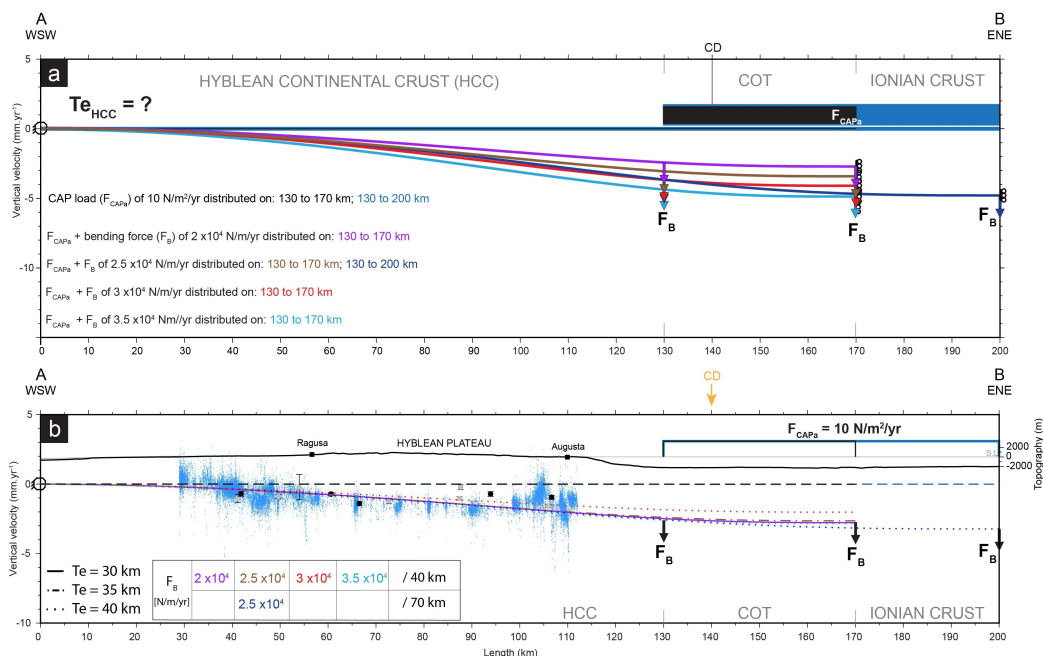
359 mum), even if significant, is not sufficient to fit the Ionian slab profile (gray line in Figures
360 5b and 5c).

361 The slab pull force is then added to the northern termination of the Ionian litho-
362 sphere as a point load (Figure 5b). Flexural models are tested with different slab pull
363 forces from 1×10^{12} to 4×10^{12} N, consistent with other publications reviewing slab rollback
364 mechanical properties (e.g., Lallemand *et al.*, 2008), and the same range of elastic thick-
365 nesses from 25 to 37 km (Figure 5c and Supplementary Figure S9). The best fit to the Cal-
366 abrian slab top is obtained for elastic thicknesses (T_e) of 27-30 km, a maximum accre-
367 tionary wedge load (F_{CAP}) of 2.5×10^8 N/m², and a slab pull force (F_{SP}) of 2×10^{12} N (Figure
368 5c and Supplementary Figure S9). It's worth noting that including the CAP load signifi-
369 cantly reduces the amplitude of the forebulge associated with slab bending, resulting in a
370 flat-and-ramp geometry similar to that of the Ionian slab.

371 **3.2 Crustal flexure along a WSW-ENE profile**

372 The impact of the Ionian subduction roll-back on the deformation of the Hyblean
373 Plateau is evaluated along the N30°E trending AB profile (Figure 5a), based on the follow-
374 ing simplifications: (1) The ongoing roll-back induces incremental changes in the slab pro-
375 file that corresponds to a southward translation and local deepening of the slab geometry.
376 (2) This results in a local incremental increase of the accretionary prism thickness. (3) Due
377 to the mechanical coupling of the Ionian slab and Hyblean lithosphere, the slab deepening
378 exerts an incremental downward force on the COT (Figure 6).

379 The effective elastic thickness of the Hyblean lithosphere is less constrainable than
380 that the Ionian lithosphere but should remain within standard values for a regular unde-
381 formed continental crust with an average geotherm. We test elastic thicknesses (T_e) rang-
382 ing from 25 to 40 km (Figure 6), assuming a uniform thickness, considering that the conti-
383 nent-ocean transition has the same elastic rigidity as the Hyblean crust and not taking into
384 account the oceanic lithosphere.



385 **Figure 6:** a) Continental crustal flexure is controlled by the retreat of the Ionian slab along the AB profile. We
 386 calculated the flexure (gFlex from Wickert, 2016) induced by the only Calabrian accretionary prism load
 387 (F_{CAPa}) of 10 N/m²/yr distributed on 1-km-long segments on the ocean-continent transition (COT) (black line),
 388 and on the adjacent Ionian crust (blue line) from the 130 to 170 km and 130 to 200 km marks of the AB pro-
 389 file, respectively. We represent best models (Supplementary Figure S10) of the CAP load and a bending
 390 force (F_B) of 2×10^4 N/m/yr (purple line), 2.5×10^4 N/m/yr (brown line), 3×10^4 N/m/yr (red line), and 3.5×10^4
 391 N/m/yr (light blue line) distributed on the COT, and of 2.5×10^4 N/m/yr (dark blue line) distributed on the COT
 392 plus into the Ionian crust. b) Best Hyblean crustal flexure models (Supplementary Figure S10) have elastic
 393 thicknesses of 30 km (continuous lines), 35 km (dotted-dashed lines), and 40 km (dotted lines). PS-InSAR
 394 velocities (in blue) and GNSS vertical velocities (NGL) with their uncertainties are stacked over 20 km (in
 395 black) and 40 km (in gray) along the AB profile (see location in Figure 2). Topographic and bathymetric pro-
 396 files are presented without vertical exaggeration (V.E.x1).

397 We first evaluate the flexural response due solely to the incremental increase of the
 398 CAP load induced by the southward migration of the slab profile, using our previous analy-
 399 sis of the bending of the Ionian slab. Based on the velocities of the GNSS stations situated
 400 in Calabria, we estimate the southward migration to 3 mm/yr, compared to a fixed Hyblean
 401 Plateau (Henriquet *et al.*, 2022). At the intersection between AB and CD profiles, at the
 402 175 km length mark in the CD profile, the Ionian slab dips $8 \pm 1^\circ$ toward the north (Hayes
 403 *et al.*, 2018) (Figure 5d). Taking into account the CAP geometry, its southward motion, and
 404 the slab geometry, we calculate a local incremental thickening of the CAP of 4×10^{-4} m/yr
 405 (equivalent to 400 m/Myr) and a resulting load (F_{CAPa}) of about 10 N/m²/yr (Figure 5d). Ap-



406 plying this load from the base of the Malta Escarpment to the eastern end of the Hyblean
407 continental crust profile results in a very slow onshore subsidence rate of 5×10^{-4} mm/yr
408 maximum, 6000 time smaller than the PS-InSAR subsidence rate measured in the same
409 area (~ 3 mm/yr).

410 We then investigate the effect of the southward Ionian slab roll-back and associated
411 downward pull on the COT. We first calculate the flexural rigidity of the oceanic lithosphere
412 (Turcotte and Schubert, 2014):

413

$$414 \quad D = \frac{ETe^3}{12(1-\nu^2)} \quad (2)$$

415 with a Young modulus (E) of 10^{11} Pa, a Poisson's ratio (ν) of 0.25, and effective elastic
416 thicknesses (Te) of 27-30 km (see 3.1). We obtain a flexural rigidity (D) of the Ionian litho-
417 sphere of $1.75\text{-}2.4 \times 10^{23}$ Pa.m³.

418 To simulate the Ionian slab retreat, we translate the slab profile southward, assum-
419 ing a slab retreat velocity of ~ 3 mm/yr (D'Agostino *et al.*, 2011) (Figure 5d). At the inter-
420 section of profiles AB and CD, this induces an incremental deepening of the Ionian slab of
421 about 4×10^{-4} m/yr (equivalent to 400 m/Myr), which defines the equivalent downward force
422 at the same location along the CD flexure profile (Turcotte and Schubert, 2014):

$$423 \quad F_B = \frac{\omega 2 D}{x^2 \left(L - \frac{x}{3}\right)} \quad (3)$$

424 with an incremental deflection (ω) of 4×10^{-4} m/yr (Figure 5d) and a flexural rigidity (D) of
425 $1.75\text{-}2.4 \times 10^{23}$ Pa.m³. The total profile length L corresponds to the point of the Hyblean
426 lithosphere where the deflection (ω) is null, ~ 200 km based on the PS-InSAR and struc-



427 tural data (Figure 6). The distance x corresponds to the point where the deflection (ω) is
428 estimated (intersection with profile CD). Considering $L = 250 \pm 50$ km and $x = 150$ km, the
429 equivalent incremental downward force is about $1\text{--}4 \times 10^4$ N/m/yr.

430 This equivalent force (F_B) is then applied on the AB profile to model, with gFlex, the
431 resulting flexure of the Hyblean crust/lithosphere. Flexural models are calculated with a no-
432 displacement boundary condition at the southwestern end of the profile (20 km west of
433 Gela) and a free displacement of a horizontally clamped boundary condition at its north-
434 eastern end (80 km East of Malta Escarpment). Flexural models are run with a fill density
435 of $2800 \text{ kg}\cdot\text{m}^{-3}$ solely for the CAP load. The downward force (F_B) and CAP load (F_{CAPa}) are
436 homogeneously distributed (on 1-km-long segments) over the 40 or 70 km long portion of
437 the AB profile corresponding to the only continent-ocean transition (COT) or to the COT
438 and adjacent Ionian crustal domain, respectively. We test different elastic thicknesses (T_e)
439 and bending force (F_B) ranging from 25 to 40 km and 1×10^4 to 4×10^4 N/m/yr, respectively
440 (Figure 6b and Supplementary Figure S10).

441 To determine the best Hyblean crustal flexure models, we first filter the PS-InSAR
442 vertical velocities (5 km stacked of the AB profile) using a 5 km width median filter with a
443 step of 1 km. Comparing the resulting long-wavelength trend of the PS-InSAR data with
444 the flexural models shows only misfits of less than 1 mm/yr. The comparison GNSS data
445 (20 km stacked of the AB profile and 5 km large median filter with a step of 1 km) shows a
446 higher misfit of less than 2.7 mm/yr due to a variable spatial density and quality of GNSS
447 stations over the Hyblean Plateau (Supplementary Figure S10c). The best models (0.4
448 mm/yr RMS PS-InSAR) have elastic thicknesses of 30 to 40 km, a CAP load plus a bend-
449 ing force ranging from 2×10^4 to 3.5×10^4 N/m/yr distributed on the 40-70 km long portion of
450 the AB profile (Figure 6b, and Supplementary Figures S10b, S10c). None of the tested
451 continental crustal flexure models reproduce the short wavelength deformations observed



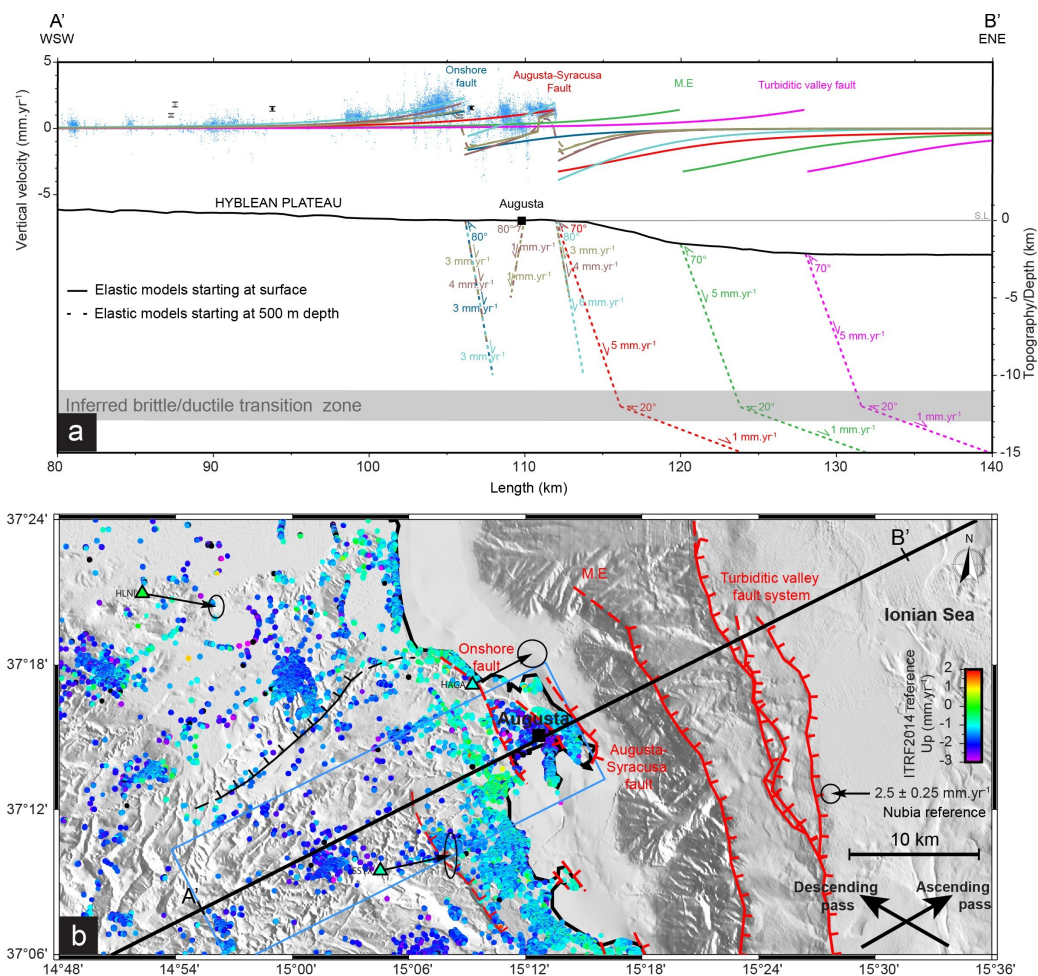
452 in the Gela region (slow uplift of ~ 0.5 mm/yr) or along the Augusta-Siracusa coastal area
453 (slower subsidence of -1 mm/yr).

454 **3.3 Interseismic loading and aseismic creep on coastal and off-shore faults**

455 Along the coast, from Augusta to Siracusa, PS-InSAR vertical velocities vary at a ki-
456 lometer scale, and appear $1-3$ mm/yr slower than the general trend of subsidence affecting
457 the Eastern Hyblean Plateau (Figures 2a and 6b). Interestingly, these short wavelength si-
458 gnals show triangular patterns similar to those produced by shallow faulting in an elastic
459 domain. To investigate the sources of these surface deformation, we test several scenarios
460 involving interseismic loading and aseismic creep on coastal and offshore faults.

461 Offshore, several active normal faults, outcropping at the base of the Malta Escarp-
462 ment, have been imaged by Gutscher *et al.* (2016) and documented in detail by Gambino
463 *et al.* (2021, 2022). Along the coastline, the Augusta-Siracusa fault (Figure 7) has been al-
464 so considered as a potential active fault (e.g., Azzaro and Barbano, 2000; Bianca *et al.*,
465 1999). We use the Coulomb 3.4 software (Toda *et al.*, 2011) to impose different fault slip
466 rates and geometric boundary conditions on these fault systems, assuming standard elas-
467 tic properties (Poisson's ratio of 0.25, Young modulus of 80 GPa).

468 The model predictions are compared to the PS-InSAR short wave-length signals
469 (Figure 7b) obtained by removing the mean of best fitting flexural models (see section 3.2)
470 from the original geodetic dataset. Two patterns of relative uplifts of about 2.5 ± 0.5 mm/yr,
471 gently tapering westward, can be identified near and to the SE of Augusta with a zone of
472 relative subsidence of about -2 ± 1 mm/yr in between them (Figure 7a). We hypothesized
473 that these surface deformations could be induced by fault slip along ENE-dipping normal
474 fault systems (Figure 7).



475 **Figure 7:** a) Coulomb 3.4 (Toda et al., 2011) numerical models of interseismic elastic loading (step of 100 m)
 476 on offshore and coastal inferred active faults along the eastern Hyblean Platform. PS-InSAR Up velocities
 477 are stacked across a 5 km width on both sides of the AB profile and appear in blue. Modeled interseismic deformations
 478 related to: the turbiditic valley normal fault identified by Gutscher et al. (2016) (magenta line); the
 479 Malta Escarpment (green line); the Augusta-Siracusa coastal fault (red line); onshore inferred active faults in
 480 Augusta (dark blue line). Modeled elastic loading of the Augusta-Siracusa coastal fault plus onshore inferred
 481 active faults in Augusta are represented in light blue, light, and dark brown lines. Topography/depth is represented
 482 without vertical exaggeration (V.E.x1). b) Map view of geodetic data in the northeastern part of the
 483 Hyblean Plateau. Major faults of the Hyblean Plateau including the Augusta-Siracusa coastal fault and the inferred
 484 onshore active fault, and Malta Escarpment (M.E) including the turbiditic valley fault identified by Gut-
 485 scher et al. (2016) and analyzed by Gambino et al. (2021, 2022) (red: active fault; red dashed: inferred active
 486 fault; black: inferred aseismic slip (Spampinato et al., 2013).

487 A first set of models corresponds to interseismic locking of the shallow (0 to 10-15
 488 km depth) sections of the main normal faults identified in the study area (Figure 7b), and
 489 elastic loading by deep (> 15 km depth) creeping sections. Regardless of the deep fault
 490 geometry or slip rates, all these models generate generalized long-wavelength subsidence



491 rates, incompatible with the geodetic data (green dotted line, Supplementary Figure S11).
492 Thus, we dismiss interseismic loading as a potential mechanisms to explain the short
493 wavelength uplift-subsidence patterns.

494 The second set of models correspond to shallow aseismic slip on three offshore
495 normal faults: the Augusta-Siracusa coastal fault (Bianca *et al.*, 1999), the Malta Escarp-
496 ment, and the turbiditic valley fault (Gutscher *et al.*, 2016; Gambino *et al.*, 2021, 2022)
497 (Figure 7a and Supplementary Figure S11). The modeled faults (Figure 7a) share a similar
498 listric geometry with a first fault plane dipping 70°NE and extending from the surface to 12
499 km depth (inferred brittle/ductile transition zone), and a second one dipping 20°NE and ex-
500 tending from 12 to 50 km depth (to limit boundary effects). We imposed slip rates of 5
501 mm/yr on the first fault plane, based on Meschis *et al.* (2020) model (Supplementary Fig-
502 ure S10), and 1 mm/yr on the second plane to dampen the elastic deformation produced
503 by slip on the shallow fault (Figure 7a). Aseismic slip on these various faults produces
504 coastal uplift rates, reaching at most ~1 mm/yr for the Augusta-Siracusa fault, consistent
505 with the PS-InSAR measurements east of Augusta (Figure 7a). However, all the modeled
506 offshore faults failed to reproduce the ~2-3 mm/yr uplift rates measured west of Augusta
507 (Figures 7a and 7b).

508 The third set of models focus on surface deformation generated by aseismic creep
509 on 70-80° ENE-dipping shallow fault planes. We first simulate slip on the upper portion of
510 the Augusta-Siracusa fault but it this model succeed in producing sufficient uplift east of
511 Augusta it failed to reproduce the observed relative uplift west of Augusta. Based on PS-
512 InSAR data, and structural evidences of onshore normal faulting (Gambino *et al.*, 2021),
513 we added to the previous Augusta-Siracusa fault model a 80° dipping onshore normal fault
514 outcropping at the 106 km mark of the AB profile, with a slip rate of 3 mm/yr down to 10 km
515 depth (light blue lines in Figure 7a). The surface deformation generated by this dual cree-
516 ping fault can explain the observed PS-InSAR relative uplift between the 103 and 106 km



517 profile marks and 110 and 112 km. Imposing aseismic slip on the onshore normal fault
518 alone fails to reproduce the subsidence east of Augusta (dark blue line in Figure 7a).

519 The triangular patterns of sharp steps and associated lows in the PS-InSAR data
520 could be also fitted by a model involving shallower aseismic creep (up to 5 to 8 km depth)
521 and combining the onshore ENE-dipping fault (106 km mark), creeping at 3-4 mm/yr, an
522 antithetic onshore WSW-dipping fault (110 km mark), creeping at 1 mm/yr, and the Augus-
523 ta-Siracusa coastal fault (112 km mark), creeping at 3-4 mm/yr (brown lines in Figure 7a).
524 This ad-hoc model illustrates that the short wavelength geodetic signal along the Eastern
525 Hyblean Plateau coast can be explained with ongoing extension tectonics and creep on
526 coastal normal faults. We test the same configuration (two onshore faults and the Augusta-
527 Siracusa coastal fault) with a fault plane propagating to the surface up to 500 m depth (Fi-
528 gure 7a). This model, equivalent to a blind fault, induces vertical surface deformation (bet-
529 ween the 106 and 110 km marks) about 0.2 mm/yr slower than the model starting to creep
530 from the surface, but still remains consistent with the PS-InSAR data.

531 **3.4 Alternative hypothesis**

532 To explore others hypothesis that could explain part of the obeserved geodetic velo-
533 city patterns, we explore three alternative models:

534 **Mantle flow upwelling**

535 Seismic tomography and volcanic data identify a slab window extending along most
536 of the northern coast of Sicily, with a slab break-off recently propagating from west to east
537 and potentially triggering toroidal and upwelling mantle flows (Civello and Margheriti, 2004;
538 Faccenna, 2005; Scarfi *et al.*, 2018; Trua *et al.*, 2003). This process could induce long
539 wavelength surface motions (so-called dynamic topography) over the whole Sicily. How-
540 ever, numerical models of the mantle flow mainly predict areas of uplift and subsidence re-
541 stricted to Mount Etna and the southern Peloritani region (Faccenna *et al.*, 2011; Gallen *et*



542 *al.*, 2023). Thus, SE Sicily appears to be situated too far from the Ionian slab edge to be
543 affected by upwelling mantle flow. It is therefore unlikely that hypothesis explains the ob-
544 served vertical surface deformation.

545 **Volcanic deflation**

546 The most recent major volcanic activity documented on the Hyblean Plateau dates
547 back 1.4 Myr (Schmincke *et al.*, 1997; Behncke, 2004), but recent minor volcanic activity,
548 not recorded at the surface, cannot be totally ruled out. In such a case, volcanic material
549 deflation located below the central Hyblean Plateau could induce local subsidence rates
550 affecting a large region. We tested this hypothesis numerically with deflating spheres (Mo-
551 gi model, Supplementary Figure S12) situated at a depth of 8 km, at the top of the Paleo-
552 zoic basement and possible location of magma accumulation (Henriquet *et al.*, 2019). Our
553 first-order tests show that even using extreme deflations of 50-75%, the PS-InSAR subsi-
554 dence rates cannot be reproduced (Supplementary Figure S12), rendering the volcanic de-
555 flation hypothesis extremely unlikely.

556 **Hydrologic loading**

557 The geology of the Hyblean Platform is mainly composed of limestones and
558 dolomites in a karstic environment. Long-term recharge or discharge of karst aquifers is
559 known to induce transient elastic deformation, measurable with geodetic data (e.g.,
560 D'Agostino *et al.*, 2018; Silverii *et al.*, 2016; Grillo *et al.*, 2011). Testing this hypothesis on
561 the Hyblean Plateau would require data and modeling of the vegetation cover, farming ac-
562 tivity, bulk volume, soil absorption capacity, etc., which is beyond the scope of the present
563 study. A detailed analysis of GNSS data could uncover such a hydrological signal, unfortu-
564 nately, the Hyblean Plateau only comprises 14 GNSS stations, of variable qualities. The
565 best-quality stations, NOT1 and HSCI show minimal pluri-annual signals potentially associ-
566 ated with hydrological variations (Supplementary Figures S2 and S4), which cannot ex-



567 plain the long wavelength trend observed over the Hyblean Plateau. Hydrologic loading, as
568 a source of large scale surface subsidence, is then unproved.

569 **4. Discussions**

570 **4.1 Short-term and long-term model limits**

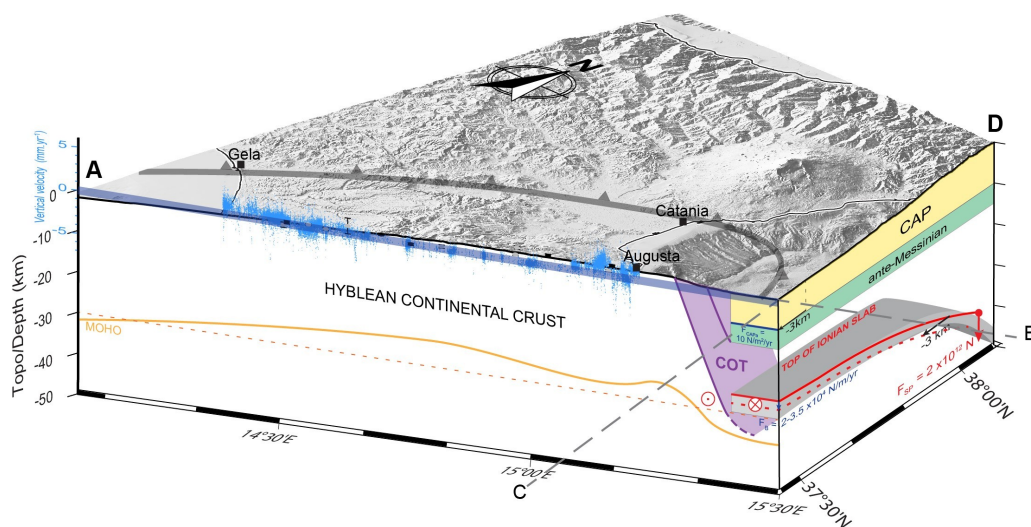
571 We explain the eastward tilt and subsidence rates of the Hyblean Plateau as the
572 flexure of the Hyblean continental crust/lithosphere induced by the southward migration of
573 the Calabrian accretionary prism (CAP) and retreat of the Ionian subducting slab (sec-
574 tions 3.1 and 3.2). This model is based on the assumption that the geodetic data (GNSS
575 and PS-InSAR) measured over a short-period (5-15 years) are representative of the kine-
576 matic evolution of the studied region at the scale of a few thousand years. Flexural model-
577 ing indicated that the increasing loading of the COT, induced by the southward propagation
578 of the CAP, is not sufficient (Figure 6b). The increase in bending force, imposed by a ~ 3
579 mm/yr southward retreat of the Ionian slab, gives interesting positive results. This process
580 could be strong enough to pull-down the Eastern termination of the Hyblean crust at veloc-
581 ities compatible with PS-InSAR measurements. However, we obtained this result consider-
582 ing that the Hyblean crust/lithosphere, the continent-ocean transition (COT), and the Ionian
583 crust/lithosphere have similar mechanical properties. This assumption implies that the
584 COT has a significantly rigid, and potentially too strong rheology (Figure 8) as discussed
585 hereafter (section 4.2).

586 We used simple 2D elastic model based on parameters determined through analyti-
587 cal modeling of the Ionian oceanic lithosphere flexure using, as a reference, the Ionian
588 slab geometry determined by Hayes *et al.* (2018). The use of more advanced numerical
589 models (FEM), including 3D modeling methods would likely improve our first-order esti-
590 mates. Similarly, the lateral variations of the Hyblean continental crust thickness and elas-



591 tic properties are not accurately known. We used the available geophysical data (Henri-
592 quet *et al.*, 2019; Scarfi *et al.*, 2018), but it was not possible to constrain the Hyblean
593 crust/lithosphere rheology with a better confidence (Figure 8). Should such parameters be-
594 come available in the future, they could be used to refine our Hyblean crust/lithosphere
595 flexure calculations.

596 One of the other assumptions we made concerns the rate of increase in the slab
597 bending force due to the southward propagation of the Ionian slab roll-back. The calcula-
598 ted increase in slab bending force east of the HP is based on the estimated rate of south-
599 ward retreat of the Ionian slab defined by the mean of the GNSS NS horizontal velocities
600 in southwest Calabria (using as a reference the Malta Island). However, this estimation
601 may be underestimated if the Calabrian Arc migrates southward slower than the Ionian
602 slab, due to its mechanical interactions with the Apulian and African margins.



603 **Figure 8:** Schematic 3D deformation model of Southeastern Sicily controlled by Ionian slab roll-back delimit-
604 ed by profiles AB and CD. The 3 km southward retreat of the Ionian crust flexure model (red dashed line) is
605 not at scale. The Moho of the Hyblean continental crust determined by geophysical data (Henriquet *et al.*,
606 2019; Scarfi *et al.*, 2018) is shown in orange. The dashed orange line represents the averaged Moho depth
607 used for flexural modeling calculations. The continent-ocean transition (COT) is shown in purple, and the
608 Calabrian accretionary prism (CAP) is shown in yellow.



609 The short-wavelength relative uplift signal, observed in the geodetic data along the
610 Southeastern Sicily coast, must be driven by more shallow deformation mechanisms than
611 those responsible for the long-wavelength eastward flexure of the HP (Figure 6b). Kilometer
612 long surface deformations are typically related to upper crustal deformation processes
613 (e.g., Burgmann and Thatcher, 2013), so we test interseismic loading models on the in-
614 ferred and identified onshore and offshore fault systems.

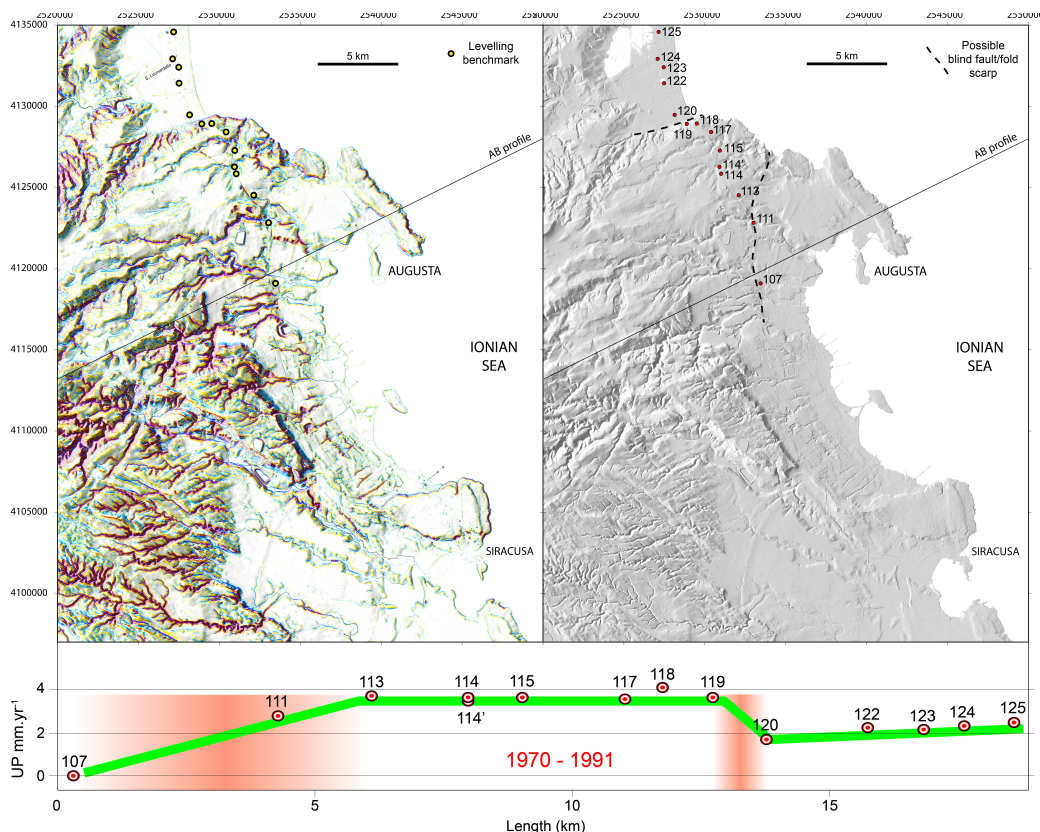
615 Slip on the Malta Escarpment and turbiditic valley normal fault (Gutscher *et al.*,
616 2016; Gambino *et al.*, 2021, 2022) cannot explain the observed deformation of the eastern
617 coast of the Hyblean Plateau. Only creep on the Augusta-Siracusa coastal fault and the
618 antithetic structure (Bianca *et al.*, 1999; Azzaro and Barbano, 2000) induce onshore verti-
619 cal deformation compatible with the geodetic data near Augusta. Interseismic slip (creep)
620 on two onshore ENE and WSW 80°-dipping faults, and the Augusta-Siracusa coastal fault
621 fits with the PS-InSAR data in the Eastern of the AB profile. These faults could be associ-
622 ated to a Triassic NW-SE graben/horst structure, the Augusta Graben, extending from Au-
623 gusta to Siracusa (e.g., Grasso and Lentini, 1982).

624 Our results suggest that these faults should creep up to the surface or the near-sur-
625 face (blind fault) to produce sufficient interseismic surface deformation in the footwall. In
626 that latter case, their surface expression could correspond to gentle surface folding or to
627 fold scarp morphologies (e.g., Chen *et al.*, 2007; Li *et al.*, 2015) rather than localized cu-
628 mulated fault scarps.

629 High precision leveling data acquired between 1970-1991 and analyzed by Spamp-
630 inato *et al.* (2013), reveals a remarkable ~4 mm/yr velocity offset between benchmarks
631 107 and 113, both situated near the coast 5 km west of Augusta (Figure 9c). This sharp
632 vertical velocity gradient is correlated with a marked topographic step, trending NS, and
633 descending toward the sea. Northwest of Augusta, the leveling dataset also shows a ~2



634 mm/yr offset between benchmarks 119 and 120, associated to a topographic step, ori-
635 ented E-W, and facing north (Figures 9b and 9c).



636 **Figure 9:** 1970-1991 leveling profile from Spampinato *et al.* (2013) performed along the Siracusa-Augusta
637 coastal domain. a) Morpho-structural map of the Augusta-Siracusa region showing fluvial incision networks
638 and morphological scarps. The location of leveling benchmarks appears in yellow circles. b) Shaded DEM
639 showing the location of leveling benchmarks with their reference numbers and potential tectonic fault/fold
640 scarps. c) 1970-1991 leveling profile showing a first velocity step (~ 4 mm/yr) between benchmark 107 and
641 113, and a second one (~ 2 mm/yr), between benchmark 119 and 120 (potential fault zone locations appear
642 in the background in red).

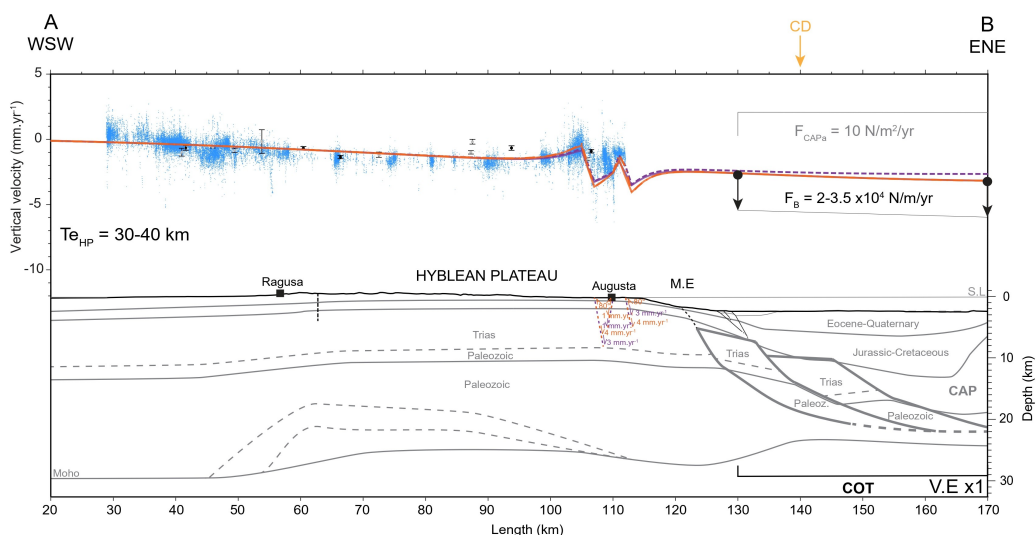
643 A morpho-structural analysis of this area, using a 5 m resolution DEM, outlines po-
644 tential drainage incision anomalies, oriented perpendicular to the identified topographic
645 steps, potentially related to tectonic surface uplift (Figure 9c). The topographic step be-
646 tween benchmarks 119 and 120 (Figures 9a and 9b) could correspond to the Scordia-
647 Lentini Graben border (e.g., Cultrera *et al.*, 2015). The topographic anomaly between
648 benchmarks 113 and 107 and extending to the north up to the Ionian Sea, and to the



649 South toward Siracusa, was not previously identified as a tectonic feature. It could corre-
650 spond to the implemented creeping fault, used to match the PS-InSAR data. Uplifted late
651 Quaternary marine terraces have been evidenced in this region (Bianca *et al.*, 1999;
652 Meschis *et al.*, 2020; Monaco and Tortorici, 2000), but the authors didn't mention a tectonic
653 origin for the measured coastal uplift. Finally, the measured fast uplift velocity (3-4 mm/yr)
654 could be considered as inconsistent with the low amplitude of the topographic scarp mea-
655 surable in the field (a few tens of meters). This point is discussed hereafter (section 4.2).

656 4.2 Combined long-term tectonics and seismic cycle model

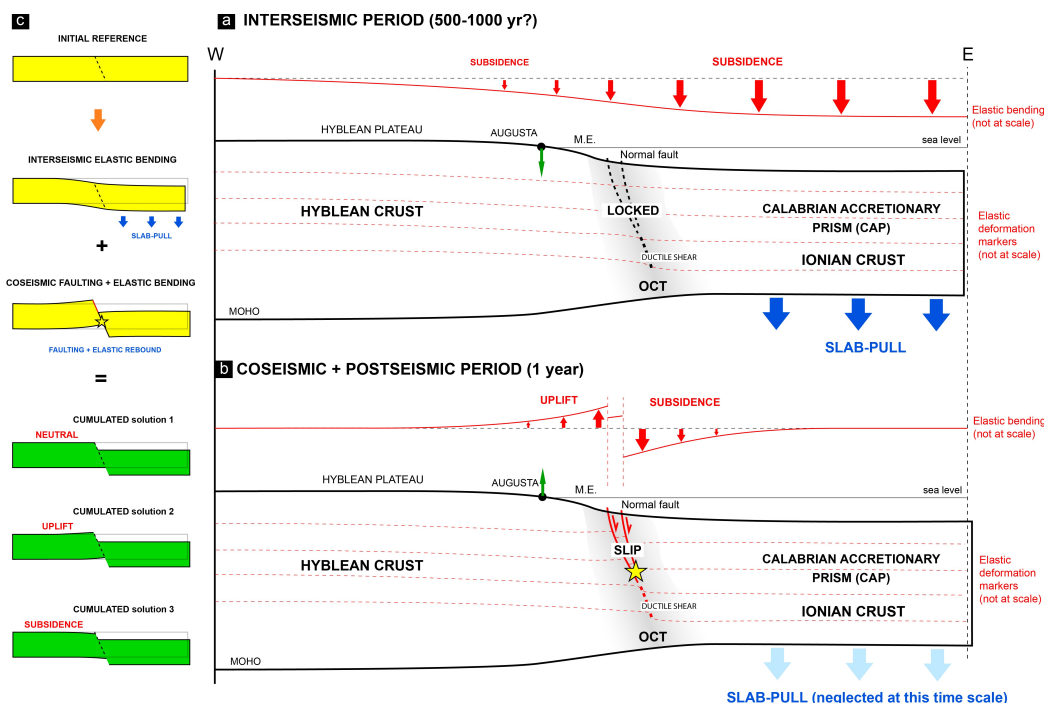
657 The subsidence and tilt patterns observed in the geodetic data can be explained by
658 the combination of (1) the flexure of the Hyblean continental crust induced by the bending
659 force associated to the Ionian subduction roll-back and the CAP overload, explaining the
660 long-wavelength deformation affecting the HP, and (2) the aseismic activity on the
661 Augusta-Siracusa fault and offshore fault bordering the eastern coast of the Hyblean
662 Plateau, explaining the short-wavelength deformation signal affecting the Augusta/Siracu-
663 sa region (Figure 10). In this section, we discuss how this short-term (geodetic) model can
664 be combined with long-term geological and tectonic observations.





665 **Figure 10** : The final model combining the possible range of the Hyblean continental crust flexural models
666 and the surface deformation (step of 1 km) induced by fault creep (from surface, continuous lines) or active
667 folding in the Augusta-Siracusa coastal domain (from 500 m, dashed lines). In this model, the flexure of the
668 Hyblean continental crust is essentially controlled by the bending force associated with the Ionian slab roll-
669 back and, to a lesser extent, by the Calabrian accretionary prism load (CAP). The synthetic structural profile
670 (gray) and topography have no vertical exaggeration (V.E.x1).

671 Initial geological analyses suggest that the eastern coast of SE Sicily has been rela-
672 tively stable over the last million year, with maximal subsidence and uplift amplitudes of
673 ± 0.2 mm/yr (Ferranti *et al.*, 2006). More recently, dating of Late Quaternary marine ter-
674 races along the Siracusa-Augusta coastal domain indicates that the eastern coast of the
675 Hyblean Plateau has experienced a slow constant uplift during the last 500 Kyr, increasing
676 northward from 0.1 to 0.4 mm/yr (Meschis *et al.*, 2020). On a shorter historical time scale
677 based on Roman archaeological site studies, Scicchitano *et al.* (2008), propose that the
678 Siracusa coast has been slowly uplifting during the last 4 Kyr, albeit with significant uncer-
679 tainties. These long-term observations, extending from the Quaternary to historical time,
680 point to a slow regional uplift, apparently in contradiction with the geodetic data. Interest-
681 ingly, along the N30°E trending AB synthetic profile, a $\sim 1^\circ$ generalized eastward tilting of
682 the HP topography can be evidenced (Figure 4a). The origin of this tilt, in apparent agree-
683 ment with the geodetic data, could be rather related to the Plio-Quaternary formation of the
684 HP (Henriquet *et al.*, 2019). To reconcile long and short time scale surface motions, we
685 propose an original seismic cycle model, driven by the southward roll-back of the Ionian
686 subduction (Figure 11).



687 **Figure 11:** Schematic model of seismic cycle for south-eastern Sicily, integrating crustal elastic bending,
 688 aseismic, and seismic faulting controlled by slab-pull. a) Interseismic period, b) coseismic and postseismic
 689 period, c) different scenarios of the cumulated interseismic, postseismic, and coseismic. This model could
 690 reconcile short and long-term observations.

691 During the interseismic phase, the active onshore and offshore normal faults affect-
 692 ing the eastern HP are locked. The Hyblean and Ionian crusts are coupled and can be
 693 compared to an elastic beam, bending eastward in response to an increasing downward
 694 vertical force: the slab pull induced by the Ionian slab roll-back (Figure 11a). Considering a
 695 minimum 500 yr return period for earthquakes such as the 1693 Val-di-Noto event (Bianca
 696 *et al.*, 1999; Meschis *et al.*, 2020), and extrapolating the PS-InSAR measurements on that
 697 period, coastal subsidence along the Siracusa-Augusta region could reach 1-2 m. This
 698 subsidence could be significantly reduced if the onshore faults, potentially related to extra-
 699 dos deformation, creep aseismically during that period. During the coseismic and postseis-
 700 mic phases, the Malta Escarpment fault unlocks, and seismic slip induces (for a $M_w > 7$



701 earthquake) multi-metric subsidence of the hanging wall and an associated decametric to
702 metric uplift of the foot-wall (e.g., Wells and Coppersmith, 1994) (Figure 11b).

703 The cumulated succession of inter-seismic coastal subsidence and co-seismic uplift
704 could result in three different scenarios (Figure 11c). If the co-seismic coastal uplift equals
705 the cumulated interseismic subsidence, the coastal domain remains stable in the long
706 term. If the former is lower than the latter, as predicted by elastic modeling (Figure 7a), the
707 coast subsides. Conversely, the coast uplifts in the long-term if coseismic uplift surpasses
708 interseismic subsidence. Considering that geological data suggest a slow coastal uplift,
709 this last scenario should be favored but additional sources of foot-wall uplift must be identi-
710 fied (Ferranti *et al.*, 2006; Meschis *et al.*, 2020). At this stage, we can only evoked raw hy-
711 pothesis:

712 - The buoyancy of the flexed Hyblean crust could significantly increase post-seismic slip
713 after major earthquakes and thus increase footwall uplift in the coastal region.

714 - Further north along the coast, the Ionian slab plunges to great depth and is certainly de-
715 tached from the Hyblean continental margin owing to a tear-fault propagation southward
716 (e.g., Gutscher *et al.*, 2016; Maesano *et al.*, 2020), which could generate additional stress
717 affecting the surface deformation of the studied region.

718 - Finally, the interseismic activity of the inferred extrado onshore faults alone could explain
719 the slow long-term uplift (0.1-0.4 mm/yr) off the eastern coast of the HP. In that case, their
720 activities should be intermittent, alternating between aseismic slip (as presently) and long
721 periods of quiescence.

722 **5. Conclusion**



723 Present-day deformation of south-eastern Sicily (Hyblean Plateau) reveals specific long
724 and short-wavelength signals indicating a generalized eastward tilt, reversing a few kilo-
725 meters before reaching the eastern coast of the Hyblean Plateau.

726 We propose that the long-wavelength tilt and subsidence can be explained by the
727 flexure of the Hyblean continental crust in response to the bending force induced by the
728 southward retreat of the Ionian subduction. Simple flexural modeling, using standard pa-
729 rameters (elastic thickness of 30-40 km, accretionary prism loading of 10 N/m²/yr, and a lo-
730 cal increase of bending force of 2-3.5 x10⁴ N/m/yr) support this interpretation.

731 We show that the short wavelength coastal signal can be explained by ongoing
732 shallow creep (at 1-4 mm/yr) of ENE trending and steeply dipping normal faults, producing
733 the local relative uplift measured geodetically. We tested other hypotheses, such as up-
734 welling mantle flow, volcanic deflation, and hydrological loading, and found them to be
735 much less plausible.

736 Finally, we proposed that surface deformation of Southeastern Sicily is mainly con-
737 trolled by bending force induced by the Ionian slab roll-back, tilting the Hyblean Plateau
738 eastward. The bending of the continental crust causes aseismic extrados deformation
739 along the eastern coast of the Hyblean Plateau while the normal faults, affecting the conti-
740 nent-ocean transition, potentially at the origin of the 1693 earthquake, remain currently
741 locked and accumulating interseismic strain. During major earthquake, the coastal domain
742 uplift and compensate the interseismic subsidence.

743 To further develop the formulated hypotheses, the acquisition of additional data is
744 mandatory, such as: new high-resolution bathymetric data, onshore and offshore seismic
745 data (CHIRP), on-site analysis to investigate inferred coastal active faults off Augusta-Sira-
746 cusa. Besides, acquiring new PS-InSAR data would improve distinguishing geological pro-
747 cesses from human activities. To further investigate these assumptions, perform more ad-
748 vanced flexural models using 3D finite element modeling techniques, and perform electri-



749 cal resistivity profile and gravimetric measurements to better constrain karstic aquifers and
750 the potential role of deep water storage and discharge on vertical surface deformation.

751 **Competing interests:**

752 The contact author has declared that none of the authors has any competing interests.

753 **Acknowledgments:**

754 This study was funded by the CNRS-INSU-Tellus programs, and the University of Montpel-
755 lier (UM). Data supporting materials can be download from the Easy Data repository
756 ([Dataterra \(easydata.earth\)](https://easydata.earth)). The maps and graphics presented in this study were generated
757 using the Generic Mapping Tools (GMT) software (Wessel and Smith, 1998). We are
758 grateful to Serge Lallemand and Nestor Cerpa for helpful discussions on flexural models of
759 the Ionian subduction.

760 **Author Contributions:**

761 Data curation: Amélie Viger, Stéphane Dominguez

762 Formal analysis: Amélie Viger, Stéphane Dominguez, Michel Peyret, Stéphane Mazzotti,
763 Maxime Henriquet, Giovanni Barreca, Carmelo Monaco, Adrien Damon

764 Funding acquisition: Stéphane Dominguez

765 Ressources: Amélie Viger, Stéphane Dominguez, Maxime Henriquet, Giovanni Barreca,
766 Carmelo Monaco

767 Software: Amélie Viger, Adrien Damon, Michel Peyret, Stéphane Mazzotti

768 Visualization: Amélie Viger, Stéphane Dominguez

769 Writing – original draft: Amélie Viger, Stéphane Dominguez



770 Writing – review and editing: Amélie Viger, Stéphane Dominguez, Michel Peyret, Stéphane
771 Mazzotti, Maxime Henriquet, Giovanni Barreca, Carmelo Monaco, Adrien Damon

772 6- References

- Altamimi, Z., Rebischung, P., Métivier, L., & Collilieux, X. (2016). ITRF2014 : A new release of the International Terrestrial Reference Frame modeling nonlinear station motions. *Journal of Geophysical Research: Solid Earth*, 121(8), 6109-6131. <https://doi.org/10.1002/2016JB013098>
- Anzidei, M., Scicchitano, G., Scardino, G., Bignami, C., Tolomei, C., Vecchio, A., Serpelloni, E., De Santis, V., Monaco, C., & Milella, M. (2021). Relative sea-level rise scenario for 2100 along the coasts of south eastern Sicily by GNSS and InSAR data, satellite images and high-resolution topography. *EGU General Assembly Conference Abstracts*, EGU21-2889. <https://ui.adsabs.harvard.edu/abs/2021EGUGA..23.2889A/abstract>
- APAT. (2005). *Carta geologica d'Italia Scala 1 : 1 250 000*. Agenzia per la Protezione dell'Ambiente e per i Servizi Tecnici-Dipartimento Difesa del Suolo, Servizio Geologico d'Italia., S.El.CA., Firenze, Italy. <https://www.isprambiente.gov.it/images/progetti/progetto-1250-ita.jpg>
- Argnani, A., Armigliato, A., Pagnoni, G., Zaniboni, F., Tinti, S., & Bonazzi, C. (2012). Active tectonics along the submarine slope of south-eastern Sicily and the source of the 11 January 1693 earthquake and tsunamis. *Natural Hazards and Earth System Sciences*, 12(5), 1311-1319. <https://doi.org/10.5194/nhess-12-1311-2012>
- Argnani, A., & Bonazzi, C. (2005). Malta Escarpment fault zone offshore eastern Sicily : Pliocene-Quaternary tectonic evolution based on new multichannel seismic data. *Tectonics*, 24(4). <https://doi.org/10.1029/2004TC001656>
- Azzaro, R., & Barbano, M. S. (2000). *Analysis of the seismicity of Southeastern Sicily : A proposed tectonic interpretation*. <https://www.earth-prints.org/handle/2122/1292>
- Behncke, B. (2004). Late Pliocene volcanic island growth and flood basalt-like lava emplacement in the Hyblean Mountains (SE Sicily) : Late Pliocene Hyblean volcanism. *Journal of Geophysical Research: Solid Earth*, 109(B9). <https://doi.org/10.1029/2003JB002937>
- Bianca, M., Monaco, C., Tortorici, L., & Cernobori, L. (1999). Quaternary normal faulting in Southeastern Sicily (Italy) : A seismic source for the 1693 large earthquake. *Geophysical Journal International*, 139(2), 370-394. <https://doi.org/10.1046/j.1365-246x.1999.00942.x>
- Bigi, G., Cosentino, D., Parlotto, M., & Sartori, R. (1991). Structural model of Italy, sheet 6, 1991. *National Council of Researches Roma*.
- Billi, A., Minelli, L., Orecchio, B., & Presti, D. (2010). Constraints to the cause of three historical tsunamis (1908, 1783, and 1693) in the Messina straits region, Sicily, southern Italy. *Seismological Research Letters*, 81(6), 907-915. <https://doi.org/10.1785/gssrl.81.6.907>
- Blewitt, G., Hammond, W., & Kreemer, C. (2018). Harnessing the GPS data explosion for interdisciplinary science. *Eos*, 99. <https://doi.org/10.1029/2018eo104623>
- Burgmann, R., & Thatcher, W. (2013). Space geodesy : A revolution in crustal deformation measurements of tectonic processes. *Special Paper of the Geological Society of America*, 500, 397-430. [https://doi.org/10.1130/2013.2500\(12\)](https://doi.org/10.1130/2013.2500(12))
- Canova, F., Tolomei, C., Salvi, S., Toscani, G., & Seno, S. (2012). Land subsidence along the Ionian coast of SE Sicily (Italy), detection and analysis via Small Baseline Subset (SBAS) multi-temporal differential SAR interferometry. *Earth Surface Processes and Landforms*, 37(3), 273-286. <https://doi.org/10.1002/esp.2238>



- Carminati, E., & Doglioni, C. (2005). Mediterranean Tectonics. In *Encyclopedia of Geology* (p. 135-146). <https://doi.org/10.1016/B0-12-369396-9/00135-0>
- Carminati, E., Lustrino, M., & Doglioni, C. (2012). Geodynamic evolution of the central and western Mediterranean: Tectonics vs. igneous petrology constraints. *Tectonophysics*, 579, 173-192. <https://doi.org/10.1016/j.tecto.2012.01.026>
- Catalano, R., Doglioni, C., & Merlini, S. (2001). On the Mesozoic Ionian Basin. *Geophysical Journal International*, 144(1), 49-64. <https://doi.org/10.1046/j.0956-540X.2000.01287.x>
- Cavallaro, D., Monaco, C., Polonia, A., Sulli, A., & Di Stefano, A. (2017). Evidence of positive tectonic inversion in the north-central sector of the Sicily Channel (Central Mediterranean). *Natural Hazards*, 86(S2), 233-251. <https://doi.org/10.1007/s11069-016-2515-6>
- Chamot-Rooke, N., Rabaute, A., & Kreemer, C. (2005). Western Mediterranean Ridge mud belt correlates with active shear strain at the prism-backstop geological contact. *Geology*, 33(11), 861. <https://doi.org/10.1130/G21469.1>
- Chen, Y.-G., Lai, K.-Y., Lee, Y.-H., Suppe, J., Chen, W.-S., Lin, Y.-N. N., Wang, Y., Hung, J.-H., & Kuo, Y.-T. (2007). Coseismic fold scarps and their kinematic behavior in the 1999 Chi-Chi earthquake Taiwan. *Journal of Geophysical Research: Solid Earth*, 112(B3). <https://doi.org/10.1029/2006JB004388>
- Civello, S., & Margheriti, L. (2004). Toroidal mantle flow around the Calabrian slab (Italy) from SKS splitting. *Geophysical Research Letters*, 31(10). <https://doi.org/10.1029/2004GL019607>
- Cloetingh, S., Ziegler, P. A., Beekman, F., Burov, E. B., Garcia-Castellanos, D., & Matenco, L. (2015). Tectonic models for the evolution of sedimentary basins. In *Treatise on Geophysics* (p. 513-592). <https://doi.org/10.1016/B978-0-444-53802-4.00117-2>
- Corti, G., Cuffaro, M., Doglioni, C., Innocenti, F., & Piero, M. (2006). Coexisting geodynamic processes in the Sicily Channel. In *Special Paper of the Geological Society of America* (Vol. 409, p. 96). [https://doi.org/10.1130/2006.2409\(05\)](https://doi.org/10.1130/2006.2409(05))
- Cultrera, F., Barreca, G., Scarfi, L., & Monaco, C. (2015). Fault reactivation by stress pattern reorganization in the Hyblean foreland domain of SE Sicily (Italy) and seismotectonic implications. *Tectonophysics*, 661, 215-228. <https://doi.org/10.1016/j.tecto.2015.08.043>
- D'Agostino, N., D'Anastasio, E., Gervasi, A., Guerra, I., Nedimović, M. R., Seeber, L., & Steckler, M. (2011). Forearc extension and slow rollback of the Calabrian Arc from GPS measurements. *Geophysical Research Letters*, 38(17). <https://doi.org/10.1029/2011GL048270>
- D'Agostino, N., Silverii, F., Amoroso, O., Convertito, V., Fiorillo, F., Ventafriida, G., & Zollo, A. (2018). Crustal deformation and seismicity modulated by groundwater recharge of karst aquifers. *Geophysical Research Letters*, 45(22), 12,253-12,262. <https://doi.org/10.1029/2018GL079794>
- Dellong, D., Klingelhoefer, F., Dannowski, A., Kopp, H., Murphy, S., Graindorge, D., Margheriti, L., Moretti, M., Barreca, G., Scarfi, L., Polonia, A., & Gutscher, M. (2020). Geometry of the deep Calabrian subduction (central Mediterranean sea) from wide-angle seismic data and 3-D gravity modeling. *Geochemistry, Geophysics, Geosystems*, 21(3), 2019GC008586. <https://doi.org/10.1029/2019GC008586>
- Dellong, D., Klingelhoefer, F., Kopp, H., Graindorge, D., Margheriti, L., Moretti, M., Murphy, S., & Gutscher, M.-A. (2018). Crustal structure of the Ionian basin and eastern Sicily margin: results from a wide-angle seismic survey. *Journal of Geophysical Research: Solid Earth*, 123(3), 2090-2114. <https://doi.org/10.1002/2017JB015312>
- Fabian, A., Bruyninx, C., Miglio, A., & Legrand, J. (2021). *M3G - Metadata Management and Distribution System for Multiple GNSS Networks*. <https://doi.org/10.24414/ROB-GNSS-M3G>
- Faccenna, C. (2005). Constraints on mantle circulation around the deforming Calabrian slab. *Geophysical Research Letters*, 32(6), L06311. <https://doi.org/10.1029/2004GL021874>
- Faccenna, C., Molin, P., Orecchio, B., Olivetti, V., Bellier, O., Funiciello, F., Minelli, L., Piromallo, C., & Billi, A. (2011). Topography of the Calabria subduction zone (southern Italy): Clues



- for the origin of Mt. Etna. *Tectonics*, 30(1), 2010TC002694. <https://doi.org/10.1029/2010TC002694>
- Ferranti, L., Antonioli, F., Anzidei, M., Monaco, C., & Stocchi, P. (2010). The timescale and spatial extent of recent vertical tectonic motions in Italy : Insights from relative sea-level changes studies. *Journal of the Virtual Explorer*, 36. <https://doi.org/10.3809/jvirtex.2010.00255>
- Ferranti, L., Antonioli, F., Mauz, B., Amorosi, A., Dai Pra, G., Mastronuzzi, G., Monaco, C., Orrù, P., Pappalardo, M., Radtke, U., Renda, P., Romano, P., Sansò, P., & Verrubbi, V. (2006). Markers of the last interglacial sea-level high stand along the coast of Italy : Tectonic implications. *Quaternary International*, 145-146, 30-54. <https://doi.org/10.1016/j.quaint.2005.07.009>
- Finetti, I. R., Lentini, F., Carbone, S., Del Ben, A., Di Stefano, A., Forlin, E., Guarnieri, P., Pipan, M., & Prizzon, A. (2005). Geological outline of Sicily and lithospheric tectono-dynamics of its Tyrrhenian margin from new CROP seismic data. *CROP Project: deep seismic exploration of the central Mediterranean and Italy*, 319-375.
- Frizon de Lamotte, D., Raulin, C., Mouchot, N., Wrobel-Daveau, J.-C., Blanpied, C., & Ringenbach, J.-C. (2011). The southernmost margin of the Tethys realm during the Mesozoic and Cenozoic : Initial geometry and timing of the inversion processes. *Tectonics*, 30(3). <https://doi.org/10.1029/2010TC002691>
- Funiciello, R., Parotto, M., Praturlon, A., & Bigi, G. (1981). Carta tettonica d'Italia alla scala 1 : 1.500. 000. *CNR Progetto Finalizzato Geodinamica, Pubbl*, 269.
- Gallen, S. F., Seymour, N. M., Glotzbach, C., Stockli, D. F., & O'Sullivan, P. (2023). Calabrian forearc uplift paced by slab–mantle interactions during subduction retreat. *Nature Geoscience*, 1-8.
- Gambino, S., Barreca, G., Gross, F., Monaco, C., Gutscher, M., & Alsop, G. I. (2022). Assessing the rate of crustal extension by 2D sequential restoration analysis : A case study from the active portion of the Malta Escarpment. *Basin Research*, 34(1), 321-341. <https://doi.org/10.1111/bre.12621>
- Gambino, S., Barreca, G., Gross, F., Monaco, C., Krastel, S., & Gutscher, M.-A. (2021). Deformation pattern of the northern sector of the Malta Escarpment (offshore SE Sicily, Italy) : Fault dimension, slip prediction, and seismotectonic implications. *Frontiers in Earth Science*, 8, 594176. <https://doi.org/10.3389/feart.2020.594176>
- Goes, S., Giardini, D., Jenny, S., Hollenstein, C., Kahle, H.-G., & Geiger, A. (2004). A recent tectonic reorganization in the south-central Mediterranean. *Earth and Planetary Science Letters*, 226(3), 335-345. <https://doi.org/10.1016/j.epsl.2004.07.038>
- Grasso, M. t., & Lentini, F. (1982). Sedimentary and tectonic evolution of the Eastern Hyblean Plateau (Southeastern Sicily) during late Cretaceous to Quaternary time. *Palaeogeography, Palaeoclimatology, Palaeoecology*, 39(3-4), 261-280.
- Grillo, B., Braitenberg, C., Devoti, R., & Nagy, I. (2011). The study of karstic aquifers by geodetic measurements in Bus de la Genziana station – Cansiglio plateau (Northeastern Italy). *Acta Carsologica*, 40(1). <https://doi.org/10.3986/ac.v40i1.35>
- Gueguen, E., Doglioni, C., & Fernandez, M. (1998). On the post-25 Ma geodynamic evolution of the western Mediterranean. *Tectonophysics*, 298(1-3), 259-269. [https://doi.org/10.1016/S0040-1951\(98\)00189-9](https://doi.org/10.1016/S0040-1951(98)00189-9)
- Gutscher, M.-A., Dominguez, S., de Lepinay, B. M., Pinheiro, L., Gallais, F., Babonneau, N., Cattaneo, A., Le Faou, Y., Barreca, G., Micallef, A., & Rovere, M. (2016). Tectonic expression of an active slab tear from high-resolution seismic and bathymetric data offshore Sicily (Ionian Sea). *Tectonics*, 35(1), 39-54. <https://doi.org/10.1002/2015TC003898>
- Gutscher, M.-A., Roger, J., Baptista, M.-A., Miranda, J. M., & Tinti, S. (2006). Source of the 1693 Catania earthquake and tsunamis (southern Italy) : New evidence from tsunami modeling of a locked subduction fault plane. *Geophysical Research Letters*, 33(8). <https://doi.org/10.1029/2005GL025442>



- Handy, M. R., M. Schmid, S., Bousquet, R., Kissling, E., & Bernoulli, D. (2010). Reconciling plate-tectonic reconstructions of Alpine Tethys with the geological–geophysical record of spreading and subduction in the Alps. *Earth-Science Reviews*, 102(3-4), 121-158. <https://doi.org/10.1016/j.earscirev.2010.06.002>
- Hayes, G. P., Moore, G. L., Portner, D. E., Hearne, M., Flamme, H., Furtney, M., & Smoczyk, G. M. (2018). Slab2, a comprehensive subduction zone geometry model. *Science*, 362(6410), 58-61. <https://doi.org/10.1126/science.aat4723>
- Henriquet, M., Dominguez, S., Barreca, G., Malavieille, J., Cadio, C., & Monaco, C. (2019). Deep origin of the dome-shaped Hyblean Plateau, Southeastern Sicily : A new tectono-magmatic model. *Tectonics*, 38(12), 4488-4515. <https://doi.org/10.1029/2019TC005548>
- Henriquet, M., Dominguez, S., Barreca, G., Malavieille, J., & Monaco, C. (2020). Structural and tectono-stratigraphic review of the Sicilian orogen and new insights from analogue modeling. *Earth-Science Reviews*, 208, 103257. <https://doi.org/10.1016/j.earscirev.2020.103257>
- Henriquet, M., Peyret, M., Dominguez, S., Barreca, G., Monaco, C., & Mazzotti, S. (2022). Present-day surface deformation of Sicily derived from Sentinel-1 InSAR time-Series. *Journal of Geophysical Research: Solid Earth*, 127(3), Article 3. <https://doi.org/10.1029/2021JB023071>
- Istituto Nazionale di Geofisica e Vulcanologia (INGV). (2005). *Rete Sismica Nazionale (RSN)*. <https://doi.org/10.13127/SD/X0FXNH7QFY>
- Kreemer, C., Blewitt, G., & Klein, E. C. (2014). A geodetic plate motion and Global Strain Rate Model. *Geochemistry, Geophysics, Geosystems*, 15(10), 3849-3889. <https://doi.org/10.1002/2014GC005407>
- Lallemand, S., Heuret, A., Faccenna, C., & Funiciello, F. (2008). Subduction dynamics as revealed by trench migration. *Tectonics*, 27(3), TC3014. <https://doi.org/10.1029/2007TC002212>
- Lentini, F., & Carbone, S. (2014). Geologia della Sicilia-geology of Sicily. *Memorie Descr. Carta Geologica d'Italia*, 95, 7-414.
- Levandowski, W., Herrmann, R. B., Briggs, R., Boyd, O., & Gold, R. (2018). An updated stress map of the continental United States reveals heterogeneous intraplate stress. *Nature Geoscience*, 11(6), 433-437. <https://doi.org/10.1038/s41561-018-0120-x>
- Li, T., Chen, J., Thompson, J. A., Burbank, D. W., & Yang, H. (2015). Hinge-migrated fold-scarp model based on an analysis of bed geometry : A study from the Mingyaole anticline, southern foreland of Chinese Tian Shan. *Journal of Geophysical Research: Solid Earth*, 120(9), 6592-6613. <https://doi.org/10.1002/2015JB012102>
- Lymer, G., Lofi, J., Gaullier, V., Maillard, A., Thinon, I., Sage, F., Chanier, F., & Vendeville, B. C. (2018). The Western Tyrrhenian Sea revisited : New evidence for a rifted basin during the Messinian Salinity Crisis. *Marine Geology*, 398, 1-21. <https://doi.org/10.1016/j.margeo.2017.12.009>
- Maesano, F. E., Tiberti, M. M., & Basili, R. (2020). Deformation and fault propagation at the lateral termination of a subduction zone : The Alfeo Fault System in the Calabrian Arc, southern Italy. *Frontiers in Earth Science*, 8, 107.
- Masson, C., Mazzotti, S., & Vernant, P. (2019). Precision of continuous GPS velocities from statistical analysis of synthetic time series. *Solid Earth*, 10(1), 329-342. <https://doi.org/10.5194/se-10-329-2019>
- Mastrolombo, B., Serpelloni, E., Argnani, A., Bonforte, A., Burgmann, R., Anzidei, M., Baldi, P., & Puglisi, G. (2014). Fast geodetic strain-rates in eastern Sicily (southern Italy) : New insights into block tectonics and seismic potential in the area of the great 1693 earthquake. *Earth and Planetary Science Letters*, 404. <https://doi.org/10.1016/j.epsl.2014.07.025>
- Mattia, M., Bruno, V., Cannavò, F., & Palano, M. (2012). Evidences of a contractional pattern along the northern rim of the Hyblean Plateau (Sicily, Italy) from GPS data. *Geologica Acta: an international earth science journal*, 10(1), 1-8.



- Mazzotti, S., James, T. S., Henton, J., & Adams, J. (2005). GPS crustal strain, postglacial rebound, and seismic hazard in eastern North America : The Saint Lawrence valley example. *Journal of Geophysical Research: Solid Earth*, 110(B11). <https://doi.org/10.1029/2004JB003590>
- Meschis, M., Scicchitano, G., Roberts, G. P., Robertson, J., Barreca, G., Monaco, C., Spampinato, C., Sahy, D., Antonioli, F., Mildon, Z. K., & Scardino, G. (2020). Regional deformation and offshore crustal local faulting as combined processes to explain uplift through time constrained by investigating differentially uplifted Late Quaternary paleoshorelines : The foreland Hyblean Plateau, SE Sicily. *Tectonics*, 39(12), e2020TC006187. <https://doi.org/10.1029/2020TC006187>
- Michael, A. J. (1984). Determination of stress from slip data : Faults and folds. *Journal of Geophysical Research: Solid Earth*, 89(B13), 11517-11526. <https://doi.org/10.1029/JB089iB13p11517>
- Milano, M., Kelemework, Y., La Manna, M., Fedi, M., Montanari, D., & Iorio, M. (2020). Crustal structure of Sicily from modelling of gravity and magnetic anomalies. *Scientific Reports*, 10(1), 16019.
- Minelli, L., & Faccenna, C. (2010). Evolution of the Calabrian accretionary wedge (central Mediterranean). *Tectonics*, 29(4). <https://doi.org/10.1029/2009TC002562>
- Mogi, K. (1958). Relations between the Eruptions of Various Volcanoes and the Deformations of the Ground Surfaces around them. *Earthq Res Inst*, 36, 99-134.
- Monaco, C., & Tortorici, L. (2000). Active faulting in the Calabrian arc and eastern Sicily. *Journal of Geodynamics*, 29(3-5), 407-424.
- Palano, M., Ferranti, L., Monaco, C., Mattia, M., Aloisi, M., Bruno, V., Cannavò, F., & Siligato, G. (2012). GPS velocity and strain fields in Sicily and southern Calabria, Italy : Updated geodetic constraints on tectonic block interaction in the central Mediterranean. *Journal of Geophysical Research: Solid Earth*, 117(B7). <https://doi.org/10.1029/2012JB009254>
- Prada, M., Sallarès, V., Ranero, C. R., Vendrell, M. G., Grevemeyer, I., Zitellini, N., & de Franco, R. (2014). Seismic structure of the Central Tyrrhenian basin : Geophysical constraints on the nature of the main crustal domains. *Journal of Geophysical Research: Solid Earth*, 119(1), 52-70.
- Rabaute, A., & Chamot-Rooke, N. (2019). Active inversion tectonics from Algiers to Sicily. In N. Sundararajan, M. Eshagh, H. Saibi, M. Meghraoui, M. Al-Garni, & B. Giroux (Éds.), *On Significant Applications of Geophysical Methods* (p. 249-251). Springer International Publishing. https://doi.org/10.1007/978-3-030-01656-2_56
- Ridente, D., Martorelli, E., Bosman, A., & Chiocci, F. L. (2014). High-resolution morpho-bathymetric imaging of the Messina Strait (Southern Italy). New insights on the 1908 earthquake and tsunami. *Geomorphology*, 208, 149-159. <https://doi.org/10.1016/j.geomorph.2013.11.021>
- Rosenbaum, G., Lister, G. S., & Duboz, C. (2002). Reconstruction of the tectonic evolution of the western Mediterranean since the Oligocene. *Journal of the Virtual Explorer*.
- Rovida, A., Locati, M., Camassi, R., Lolli, B., Gasperini, P., & Antonucci, A. (2022). *Catálogo Parametrico dei Terremoti Italiani (CPTI15), versione 4.0* (4.0, p. 4894 earthquakes). Istituto Nazionale di Geofisica e Vulcanologia (INGV). <https://doi.org/10.13127/CPTI/CPTI15.4>
- Scandone, P., Patacca, E., Radoicic, R., Ryan, W. B. F., Cita, M. B., Rawson, M., Chezar, H., Miller, E., McKenzie, J., & Rossi, S. (1981). Mesozoic and Cenozoic rocks from Malta escarpment (central Mediterranean). *AAPG Bulletin*, 65(7), 1299-1319.
- Scarfi, L., Barberi, G., Barreca, G., Cannavò, F., Koulakov, I., & Patané, D. (2018). Slab narrowing in the Central Mediterranean : The Calabro-Ionian subduction zone as imaged by high resolution seismic tomography. *Scientific Reports*, 8(1), Article 1. <https://doi.org/10.1038/s41598-018-23543-8>



- Schmincke, H.-U., Behncke, B., Grasso, M., & Raffi, S. (1997). Evolution of the northwestern Iblean Mountains, Sicily: Uplift, Pliocene/Pleistocene sea-level changes, paleoenvironment, and volcanism. *Geologische Rundschau*, 86, 637-669.
- Scicchitano, G., Antonioli, F., Berlinghieri, E. F. C., Dutton, A., & Monaco, C. (2008). Submerged archaeological sites along the Ionian coast of Southeastern Sicily (Italy) and implications for the Holocene relative sea-level change. *Quaternary Research*, 70(1), 26-39. <https://doi.org/10.1016/j.yqres.2008.03.008>
- Scicchitano, G., Gambino, S., Scardino, G., Barreca, G., Gross, F., Mastronuzzi, G., & Monaco, C. (2022). The enigmatic 1693 AD tsunamis in the eastern Mediterranean Sea: New insights on the triggering mechanisms and propagation dynamics. *Scientific Reports*, 12(1), 9573. <https://doi.org/10.1038/s41598-022-13538-x>
- Scognamiglio, L., Tinti, E., & Quintiliani, M. (2006). *Time Domain Moment Tensor (TDMT)* [jeu de données]. Istituto Nazionale di Geofisica e Vulcanologia (INGV). <https://doi.org/10.13127/TDMT>
- Sgroi, T., De Nardis, R., & Lavecchia, G. (2012). Crustal structure and seismotectonics of central Sicily (southern Italy): New constraints from instrumental seismicity: Seismotectonics of central Sicily. *Geophysical Journal International*, 189(3), 1237-1252. <https://doi.org/10.1111/j.1365-246X.2012.05392.x>
- Silverii, F., D'Agostino, N., Métois, M., Fiorillo, F., & Ventafridda, G. (2016). Transient deformation of karst aquifers due to seasonal and multiyear groundwater variations observed by GPS in southern Apennines (Italy). *Journal of Geophysical Research: Solid Earth*, 121(11), 8315-8337. <https://doi.org/10.1002/2016JB013361>
- Spampinato, C. R., Braitenberg, C., Monaco, C., & Scicchitano, G. (2013). Analysis of vertical movements in eastern Sicily and southern Calabria (Italy) through geodetic leveling data. *Journal of Geodynamics*, 66, 1-12. <https://doi.org/10.1016/j.jog.2012.12.002>
- Speranza, F., Minelli, L., Pignatelli, A., & Chiappini, M. (2012). The Ionian Sea: The oldest in situ ocean fragment of the world?: MAGNETIC MODELLING OF THE IONIAN SEA. *Journal of Geophysical Research: Solid Earth*, 117(B12), n/a-n/a. <https://doi.org/10.1029/2012JB009475>
- Stampfli, G. M., Borel, G. D., Marchant, R., & Mosar, J. (2002). Western Alps geological constraints on western Tethyan reconstructions. *Journal of the Virtual Explorer*, 08. <https://doi.org/10.3809/jvirtex.2002.00057>
- Stephenson, O. L., Liu, Y.-K., Yunjun, Z., Simons, M., Rosen, P., & Xu, X. (2022). The Impact of Plate Motions on Long-Wavelength InSAR-Derived Velocity Fields. *Geophysical Research Letters*, 49(21), e2022GL099835. <https://doi.org/10.1029/2022GL099835>
- Tesauro, M., Audet, P., Kaban, M. K., Bürgmann, R., & Cloetingh, S. (2012). The effective elastic thickness of the continental lithosphere: Comparison between rheological and inverse approaches. *Geochemistry, Geophysics, Geosystems*, 13(9). <https://doi.org/10.1029/2012GC004162>
- Toda, S., Stein, R. S., Sevilgen, V., & Lin, J. (2011). Coulomb 3.3 Graphic-rich deformation and stress-change software for earthquake, tectonic, and volcano research and teaching—User guide. *US Geological Survey open-file report*, 1060(2011), 63.
- Trua, T., Serri, G., & Marani, M. P. (2003). Lateral flow of African mantle below the nearby Tyrrhenian plate: Geochemical evidence. *Terra Nova*, 15(6), 433-440. <https://doi.org/10.1046/j.1365-3121.2003.00509.x>
- Tugend, J., Chamot-Rooke, N., Arsenikos, S., Blanpied, C., & Frizon De Lamotte, D. (2019). Geology of the Ionian Basin and Margins: A Key to the East Mediterranean Geodynamics. *Tectonics*, 38(8), 2668-2702. <https://doi.org/10.1029/2018TC005472>
- Turcotte, D. L., & Schubert, G. (2014). *Geodynamics* (Third edition). Cambridge University Press.
- Van Hinsbergen, D. J. J., Torsvik, T. H., Schmid, S. M., Mañenco, L. C., Maffione, M., Vissers, R. L. M., Gürer, D., & Spakman, W. (2020). Orogenic architecture of the Mediterranean region



- and kinematic reconstruction of its tectonic evolution since the Triassic. *Gondwana Research*, 81, 79-229. <https://doi.org/10.1016/j.gr.2019.07.009>
- Vavryčuk, V. (2014). Iterative joint inversion for stress and fault orientations from focal mechanisms. *Geophysical Journal International*, 199(1), 69-77. <https://doi.org/10.1093/gji/ggu224>
- ViDEPI. (s. d.). <https://www.videpi.com/videpi/videpi.asp>
- Vilardo, G., Ventura, G., Terranova, C., Matano, F., & Nardò, S. (2009). Ground deformation due to tectonic, hydrothermal, gravity, hydrogeological, and anthropic processes in the Campania Region (Southern Italy) from Permanent Scatterers Synthetic Aperture Radar Interferometry. *Remote Sensing of Environment*, 113(1), 197-212. <https://doi.org/10.1016/j.rse.2008.09.007>
- Vollrath, A., Zucca, F., Bekaert, D., Bonforte, A., Guglielmino, F., Hooper, A., & Stramondo, S. (2017). Decomposing DInSAR time-series into 3-D in combination with GPS in the case of low strain rates : An application to the Hyblean Plateau, Sicily, Italy. *Remote Sensing*, 9(1), 33. <https://doi.org/10.3390/rs9010033>
- Watts, A. B., & Zhong, S. (2000). Observations of flexure and the rheology of oceanic lithosphere. *Geophysical Journal International*, 142(3), 855-875.
- Wells, D. L., & Coppersmith, K. J. (1994). New empirical relationships among magnitude, rupture length, rupture width, rupture area, and surface displacement. *Bulletin of the seismological Society of America*, 84(4), 974-1002.
- Wessel, P., & Smith, W. H. F. (1998). New, improved version of generic mapping tools released. *Eos, Transactions American Geophysical Union*, 79(47), 579-579. <https://doi.org/10.1029/98EO00426>
- Wickert, A. D. (2016). Open-source modular solutions for flexural isostasy : gFlex v1.0. *Geoscientific Model Development*, 9(3), 997-1017. <https://doi.org/10.5194/gmd-9-997-2016>
- Wortel, M. J. R., & Spakman, W. (2000). Subduction and Slab Detachment in the Mediterranean-Carpathian Region. *Science*, 290(5498), 1910-1917. <https://doi.org/10.1126/science.290.5498.1910>